AD-A119 408 DAYTON UNIV OH RESEARCH INST F/G 20/4
A MODEL FOR PREDICTION BIRD AND ICE IMPACT LOADS ON STRUCTURES.(U)
MAY 82 L I BOEHMAN, A CHALLITA F33615-77-C-5221
UNCLASSIFIED UDR-TR-79-54 AFWAL-TR-82-2046 NL

(12)

AFWAL-TR-82-2046

A MODEL FOR PREDICTION BIRD AND ICE IMPACT LOADS ON STRUCTURES

L. I. BOEHMAN
A. CHALLITA

UNIVERSITY OF DAYTON RESEARCH INSTITUTE
DAYTON, OHIO 45469

MAY 1982

INTERIM REPORT FOR PERIOD 1 OCTOBER 1977 - 1 NOVEMBER 1979

APPROVED FOR PUBLIC RELEASE; DISTRIBUTION UNLIMITED

AERO PROPULSION LABORATORY
AIR FORCE WRIGHT AERONAUTICAL LABORATORIES
AIR FORCE SYSTEMS COMMAND
WRIGHT-PATTERSON AIR FORCE BASE, OHIO 45433

NOTICE

When Government drawings, specifications, or other data are used for any purpose other than in connection with a definitely related Government procurement operation, the United States Government thereby incurs no responsibility nor any obligation whatsoever; and the fact that the government may have formulated, furnished, or in any way supplied the said drawings, specifications, or other data, is not to be regarded by implication or otherwise as in any manner licensing the holder or any other person or corporation, or conveying any rights or permission to manufacture use, or sell any patented invention that may in any way be related thereto.

This report has been reviewed by the Office of Public Affairs (ASD/PA) and is releasable to the National Technical Information Service (NTIS). At NTIS, it will be available to the general public, including foreign nations.

This technical report has been reviewed and is approved for publication.

Sandra K. Drake

SANDRA K. DRAKE
Project Engineer

Isak J. Gershon

ISAK J. GERSHON
Technical Area Manager,
Propulsion Mechanical Design

FOR THE COMMANDER

James M. Shipman

J. SHIPMAN, MAJ, USAF
Deputy Director, Turbine Engine Division

If your address has changed, if you wish to be removed from our mailing list, or if the addressee is no longer employed by your organization please notify AFWAL/POTA, W-PAFB, OH 45433 to help us maintain a current mailing list .

Copies of this report should not be returned unless return is required by security considerations, contractual obligations, or notice on a specific document.

UNCLASSIFIED

SECURITY CLASSIFICATION OF THIS PAGE (When Data Entered)

REPORT DOCUMENTATION PAGE	READ INSTRUCTIONS BEFORE COMPLETING FORM
1. REPORT NUMBER: AFWAL-TR-82-2046	2. GOVT ACCESSION NO.: AD-A129408
	3. RECIPIENT'S CATALOG NUMBER
4. TITLE (and Subtitle): A MODEL FOR PREDICTING BIRD AND ICE IMPACT LOADS ON STRUCTURES	5. TYPE OF REPORT & PERIOD COVERED: Interim Report - 1 Oct. 77 - 31 Nov. 79
	6. PERFORMING ORG. REPORT NUMBER: UDR-TR-79-54
7. AUTHOR(s): L. I. Boehman, A. Challita	8. CONTRACT OR GRANT NUMBER(s): 200-FBA-14K-47844 (GE), F33615-77-C-5221
9. PERFORMING ORGANIZATION NAME AND ADDRESS: University of Dayton Research Institute, 300 College Park Ave., Cayton, Ohio 45469	10. PROGRAM ELEMENT, PROJECT, TASK AREA & WORK UNIT NUMBERS: 62203F, 3066, 12, 33
11. CONTROLLING OFFICE NAME AND ADDRESS: General Electric, Advanced Engineering and Tech. Prog. Dept., Cincinnati, Ohio 45433	12. REPORT DATE: May 1982
	13. NUMBER OF PAGES: 86
14. MONITORING AGENCY NAME & ADDRESS(if different from Controlling Office): Aero Propulsion Laboratory (AFWAL/POTC), Air Force Aeronautical Laboratories (AFSC), Wright-Patterson AFB, Ohio 45433	15. SECURITY CLASS. (of this report): UNCLASSIFIED
	15a. DECLASSIFICATION/DOWNGRADING SCHEDULE

16. DISTRIBUTION STATEMENT (of this Report)

Approved for public release; distribution unlimited.

17. DISTRIBUTION STATEMENT (of the abstract entered in Block 20, if different from Report)

18. SUPPLEMENTARY NOTES

19. KEY WORDS (Continue on reverse side if necessary and identify by block number)

Loading model, engine blade, slicing, onset flow, pressure distribution

20. ABSTRACT (Continue on reverse side if necessary and identify by block number)

This report describes a loading model for computation of the pressure distribution exerted on surfaces during bird and ice impacts. Bird and ice impacts are considered as fluid dynamic in nature and are modeled as fluid jets impinging on arbitrarily shaped three dimensional deformable surfaces. A quasi-steady, potential flow analysis is applied to the jet impact problem thereby reducing the impact problem to the problem of solving Laplace's equation. The surface simgularity technique is used to solve Laplace's —>cont

DD FORM 1 JAN 73 1473 EDITION OF 1 NOV 65 IS OBSOLETE

UNCLASSIFIED

SECURITY CLASSIFICATION OF THIS PAGE (When Data Entered)

equation.

A computer program for computing pressure distributions on both rotating and non-rotating turbine engine components is both rotating and non-rotating turbine engine components is described. Amodel for treating slicing of birds and ice by rotating blades is incorporated into this computer program. The loading model computer program is specificallu developed to be interfaced with finite-element structural analysis computer programs. Given the instantaneous impacted surface shape and displacement velocity the loading model computer program computes the pressure distribution existing on the impacted surface. The shape of the impact surface is fed to the loading modal in the loading model in the form of finite element surface nodal computer program constructs a system of quadrilateral elements covering the impacted surface. The shape of the impact surface is fed to the loading model in the form of finite element surface nodal point coordinates. From this information, the loading model computer program constructs a system of quadrilateral elements covering the impacted surface. A uniform distribution of fluid dynamic sources of unkown but determinable strength is applied to each of these quadrilateral elements. The strength of each source distribution is determined from boundary condition considerations. The jet velocity field and the pressure distribution are ultimately determined from the velocity field induced by the distribution of sources over the impact surface combined with the jet velocity field which would exist without the presence of the impacted surface.

An abbreviated user's guide is included in the report which describes the input information required to operate the loading model computer program. Bird, ice sphere, or slab ice impacts can be selected by the user. A limited number of comparisons between loading model computer pressure distribution and measured impact pressures are also included in the report.

FOREWORD

This report describes a contractual work effort conducted for the General Electric Company, Aircraft Engine Group under Purchase Order No. 200-FBA-17K-47844 which is a subcontract of F33615-77-C-5221. The prime contract is funded by the United States Air Force Aero-Propulsion Laboratory.

This report covers work conducted during the period of October 1977 to November 1979 and is part of Task IIIC.

The GE Program Manager was Mr. Joe McKenzie and the Principal Investigator was Mr. Al Storace. The work reported herein was performed under the direction of Dr. Louis I. Boehman of the Mechanical Engineering Department and Mr. Antonios Challita of the Experimental and Applied Mechanics Division, University of Dayton Research Institute.

Program management for the University was provided by Mr. Robert Bertke.

This report covers work conducted for project 3066, task 12, entitled Foreign Object Impact Design Criteria. The contract was sponsered by the Aero Propulsion Laboratory, Air Force Systems Command, Wright-Patterson AFB, Ohio 45433 under the direction of Sandra K. Drake (AFWAL/POTA), Project Engineer.

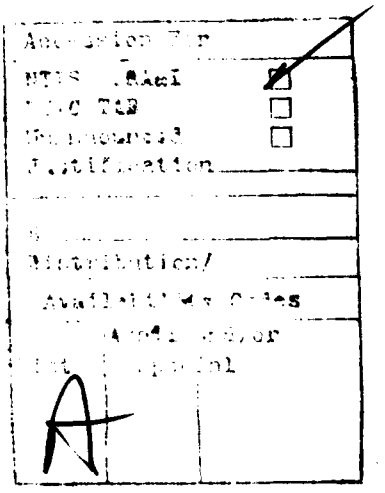

TABLE OF CONTENTS

TABLE OF CONTENTS (CONCLUDED)

LIST OF ILLUSTRATIONS

LIST OF ILLUSTRATIONS (CONCLUDED)

LIST OF TABLES

A MODEL FOR PREDICTING BIRD AND ICE IMPACT LOADS ON STRUCTURES

SECTION 1
INTRODUCTION AND SUMMARY

1.1 BACKGROUND

Hail, ice sheets, and birds are periodically ingested into aircraft engines during take-off, flight, and landing operations. The resulting damage to aircraft components such as engine fan blades and aircraft windshields can lead to destruction of the aircraft and crew. One of the most serious threats, especially in high speed flight at low altitudes, is bird ingestion into the engine. The elements of a jet engine which are most vulnerable to impact of ice and birds [foreign object damage (FOD)] are the first-stage fan blades. Conventional jet engines currently use sustain relatively minor damage with only rare occurrences of catastrophic failure when birds or ice are ingested. The first stages of these engines have "thick" titanium or stainless steel blades and run at moderate rotational speeds (chiefly limited by the strength-to-weight ratio of the blade materials). However, advanced engines currently under development require thin blades with sharp leading edges and high rotational speeds in order to obtain high speed aerodynamic efficiency. Efforts to increase the performance of conventional engines envision the use of lightweight composite materials to achieve higher rotational fan speeds and higher power-to-weight ratios. Both of these directions in fan jet engine evolution pose severe design problems for the successful development of a new generation of FOD-resistant fan blades.

Progress in the development of FOD-resistant fan blades has been hindered by the lack of understanding of the mechanisms of FOD failure, and the lack of a blade analysis tool capable of predicting the response of a fan blade to ice and bird impact

loading. The recent development of sophisticated dynamic structural analysis programs based on the finite-element methodology gives the fan blade designer the basic tool needed to determine structural response due to impact loading. What is still required, in order to use and capitalize on the power of these well-developed finite-element computer codes for blade analysis, is a physically correct and accurate model for the bird or ice impact process.

This report describes the development of a bird and ice impact loading model which is specifically designed to be used with finite-element structural analysis computer codes. Two recent developments from FOD investigations have provided the information sorely needed to obtain a fundamental understanding of the FOD impact process. The first, and most important, observation is that bird and ice impacts are primarily fluid dynamic in nature and that viscous effects can be ignored. The second observation, which is particularly important for modelling impacts on fan blades, has to do with the cutting action of a blade during the slicing of the impacting object by the leading edge of a blade. It was observed that no significant loading is attributable to the cutting action itself; that is, the slicing force is primarily due to the change in direction which the blade imparts to the slice mass. This second observation basically means that the entire impact process of a bird, hail, or slab of ice striking a fan blade can be reasonably modelled by the methods of fluid dynamic analysis without having to consider the tensile or compressive strength of the impacting object.[1]

Because the model for bird and ice impact loading described in this report is specifically designed to interface with finite element transient structural analysis computer codes, the model capitalizes on the fact that the impacted surface is fully described mathematically in the structural analysis code at any instant of time. This fact, coupled with the observation that the impact process can be modelled as an ideal (non-viscous) fluid flowing onto the blade surface suggests that the well-developed

methods of ideal fluid dynamic analysis (potential flow theory) can be used to model FOD impacts and that, in particular, the surface singularity method for solving complex potential flows is the ideal tool to be used for the impact loading model.

This report describes how the surface singularity technique is used to compute the loads exerted on a surface during FOD impacts, and how this technique interfaces with the finite-element structural analysis method. It should be mentioned here, at the outset, that the FOD loading model described in this report is not based on mathematically exact solutions to a well posed potential flow problem. Rather, because of computer time and memory limitations, only an approximate solution is obtained to model equations. The equations only approximate the true fluid dynamic event.

The overall model, while not stated or solved with exact mathematical rigor, does include descriptions of the most important physical phenomena associated with FOD impacts. These physical phenomena include the following:

1. A true three-dimensional treatment of the impact process is utilized.
2. The shape and size (i.e., geometry) of the slice mass is computed.
3. The impacted surface shape is arbitrary and deformation under load is considered (i.e., coupling between the loading process and target response is treated in a physically meaningful manner).
4. Initiation, duration, and termination of the loading process is described with separate descriptions used for birds, ice spheres, and ice slabs.

In the remainder of Section I of this report, the approximations used in the formulation of the loading model are discussed and justified. Section II describes the methods and analysis used to generate a description of the slicing process and how the slicing process is viewed and modelled for birds, ice spheres, and ice slabs impacts. Section III of the report describes the surface

singularity technique and how it is applied in the loading model. Section IV is basically a description of an FOD loading model computer program, and how it is interfaced with the finite-element structural analysis method.

1.2 FLUID DYNAMIC NATURE OF FOD IMPACTS

The impact of a bird or a slab of ice onto a jet engine fan blade is a rather unusual impact problem. It involves a number of effects that are normally avoided in impact investigations. Firstly, all bird and ice impacts on jet engine fan blades are oblique. Obliquity has the effect of making the problem three-dimensional. Only under very severe limitations ("spherical" birds or ice and nondeforming targets) can the process be reduced to two dimensions. The rigorous analysis of most truly three-dimensional impact events appears to be beyond the current state of the art. The only analytic techniques which promise to be capable of addressing general oblique impacts are finite difference methods. At the moment they are prohibitively expensive and only moderately accurate. The second important effect in bird and ice impacts with fan blades is that, in general, the impact is a slicing, edge impact. This effect ensures three-dimensionality, even under the assumptions which render oblique impacts on a plane surface two dimensional. There appear to be no proven, existing analytic techniques capable of rigorously treating an oblique, slicing edge impact. The problem must be treated with some degree of approximation. When compliant targets are considered, the degree of approximation required to obtain a solution increases. This section of the report describes an approach to the solution of this problem which incorporates rigorously the fluid dynamic nature of the impact event.

It is known from several other studies[1,2] that a material like gelatin with 10 percent porosity adequately simulates the impact properties of real birds. The early efforts in the development of the substitute bird material for use in bird-impact studies were reported by Allcock and Collin.[2]

Wilbeck[1] theoretically and experimentally studied the impact behavior of low-strength projectile materials which he characterized as soft-body materials. These materials have a much lower strength than that of typical target materials. An impact involving a projectile of soft-body material against a target surface made of aluminum or steel generates stresses that substantially exceed the strength of the projectile material but are well below the strength of the target material.

Wilbeck[1] and Barber[3] have established in their reports that, unlike impacts involving projectiles of strong materials, the impact of projectiles of soft-body materials is dominated by the tendency of the projectile material to behave like a fluid during the impact. Such soft-body materials include, in addition to bird and substitute bird materials, ice in the form of hail or ice sheets which break off the engine nacelle.

It is useful to review here the rationale for considering bird and ice impacts as fluid dynamic phenomena. Recognition of this type of behavior greatly aids in the development of a theoretical understanding of the impact process.

1.2.1 Observations Based on Experimental Measurements

Wilbeck[1] treated the impact of a bird on a rigid plate as an unsteady fluid dynamic process and developed a simplified one-dimensional analysis of a homogeneous right-circular cylinder of soft-body material impacting normally on a rigid plate. The analysis showed the entire impact process to occur in four distinct phases. In the first phase, which is the initial impact phase, very high shock, or Hugoniot, pressures are generated. He calculated this pressure, using the Hugoniot relation for a mixture, together with the shock properties of gelatin. The results of the peak pressure measurements for the impact of right circular cylinders of gelatin with 10 percent porosity reported by Barber, et al.[3] showed that the measured pressures were in good agreement with the impact pressures calculated by Wilbeck. More recent work by Bauer and Barber[4,5] shows even better agreement. This agreement in the initial phase of the

impact process indicates that the hydrodynamic description of the event is well justified.

After the first phase, the high shock pressures decay to steady fluid dynamic pressures. These pressures can be calculated by considering the process as steady jet flow. This theoretical conclusion is again in agreement with measured steady-flow pressures.[1,3,5]

Furthermore, the calculations of shock decay by Wilbeck[1] have established that for a projectile with a length-to-diameter ratio larger than a critical value, the shock will be severely weakened by radial expansion waves and the projectile should undergo complete shock decay to steady flow. Steady flow would be expected to prevail if the length-to-diameter ratio of the projectile in the direction of the impact exceeds approximately unity. For real birds striking end-on, the length-to-diameter ratio ranges from 2 to 3 and a steady-flow regime should occur. This conclusion has been amply supported by the measurements.[1,3,5]

Further evidence of the tendency of the projectile material to flow radially outward at the impact location is apparent during the steady-flow phase. As the radial pressures decrease during the shock decay, shear stresses develop in the projectile material. If the shear strength of the projectile material is large enough to withstand these shear stresses, the radial motion of the projectile will be impeded. On the other hand, the projectile material will begin to flow if its shear strength is smaller than the shear stresses developed. The experiments have confirmed that for real birds, gelatin and ice, the shear strength is low enough for the pressures generated to cause the projectile material to flow.

1.2.2 Simplified Potential Flow Model and Comparisons Of Predicted and Measured Steady-State Pressure Distributions

The absence of any entrainment of the surrounding fluid (air) during the impact process led to the recognition

that the steady-flow phase of the bird impact would be ideally suited for modeling by potential flow theory. This, in turn, led to the development of a three-dimensional potential flow model[3] for predicting the pressure distribution produced by the steady flow of a cylindrical jet impacting obliquely on a flat plate. The solution of the three-dimensional Laplace's equation for a steady, incompressible, irrotational flow was obtained by the superposition of the two elementary solutions. These elementary solutions were the uniform flow of a fluid in a round duct, and the uniform distribution of planar sources over the elliptical area on the target defined by the intersections of the round duct and the flat plate. The details of this procedure, which is an elementary application of the surface singularity technique, are described in Reference 3.

The predicted steady-flow pressure distribution calculated showed very good agreement with the measured values over the central portions of the jet flow.[3] However, the agreement was rather poor near the edges of the jet, and this descrepancy was essentially due to the fact that the vorticity effects which are important at the edges of the jet are not properly modelled by the simple superposition of two elementary potential flow solutions. Nevertheless, the fact that this simple model correctly predicted pressure distributions over the major, and most important, region of the impact zone for a wide range of impact angles further supports the concept that bird and ice impacts are essentially ideal fluid flow in nature.

1.3 ASSUMPTIONS AND THEIR JUSTIFICATIONS

It is clear from the foregoing that the impact of soft-body materials such as birds, realistic substitute bird materials like gelatin, and ice at the typical velocities of impact may be analyzed within the framework of hydrodynamic theory. The impact process is modelled in terms of normal and oblique impact of a right circular cylinder against rigid and compliant target surfaces. The theoretical analysis, of course, requires several simplifying assumptions.

The projectile material is considered to be homogeneous even when large amounts of porosity are considered. This assumption would appear to be somewhat unrealistic in the case of real birds, although extensive test data do not indicate gross inhomogeneties.[3] The assumption is quite reasonable for the substitute material (gelatin with 10 percent microballoon) and ice.

In the analysis of the impact process, the strength of the projectile material is considered to be negligible. This assumption is reasonable for the typical projectile and target materials of interest at the impact velocities of interest.

It is assumed that, at least as a first approximation, the fluid flow may be treated as incompressible. This is a reasonable assumption in view of the fact that the measured steady-state pressures are quite small in comparison to the pressures required to produce significant density changes in water.

In modeling the steady-flow phase by potential flow analysis, it is assumed that the flow is inviscid and irrotational. Since the impact process does not entail any entrainment of the surrounding fluid, and since the time over which steady flow exists is small compared to the time required to establish strong vorticity in the flow, it seems reasonable to treat the flow field as effectively irrotational, at least over the central portion of the jet. However, the fact that this simplification fails to model adequately the edges of the jet is well-recognized.

It must be noted that the presence of a significant amount of porosity in birds results in a very low sonic velocity (of the order of 40 m/s for gelatin with 10 percent porosity). Then, for the typical velocities at which bird impact occurs, the initial impact process will be largely supersonic. Thus, while the shock wave is weakened by the release waves and is ultimately eliminated for a subsonic impact, it will not disappear for a supersonic impact. The shock propagation velocity will decrease until it becomes equal to the impact velocity, then a standing shock will be established. Behind this shock the flow will be subsonic

and will follow steady flow streamlines. Wilbeck's calculations[1], based upon potential flow theory for a supersonic bird impact at normal incidence, show that the steady-flow pressure at the center of impact is almost independent of porosity, suggesting that the decrease in density due to porosity is offset by the increase in compressibility.

1.4 SUMMARY DESCRIPTION OF LOADING MODEL

If the target deforms locally during the impact, as well as translating and rotating, then a loading model capable of generating the local distribution of loading pressures during the impact is required. As described previously, birds behave like a fluid during impact and the distribution of surface pressure during impact is directly related to the fluid nature of the event. To successfully predict the surface pressure distributions on deforming surfaces, it is necessary to utilize a fundamental fluid dynamic approach. The shear stress distributions, due to boundary layer (viscous) effects can safely be ignored for both normal and oblique impacts since the ratio of maximum normal stress (pressure) to maximum shear stress is of the order of one over the skin friction coefficient. Therefore, the problem is reduced to determining the pressure distribution over the impact area.

If the event is assumed to be dominated by the quasi-steady flow portions of the impact, as described previously, the process can be thought of as the flow of a jet onto a surface as illustrated in Figure 1. (Shock effects, if demonstrated to be important, can be evaluated separately and superimposed on the quasi-steady flow results.)

The characteristic (and maximum) pressure in quasi-steady fluid flow is the Bernoullian stagnation pressure ($1/2\ \rho V_r^2$) and the important independent parameters are the impactor density, ρ, and the impact velocity, V_r. The loads are specified if the stagnation pressure and pressure coefficient distribution can be determined. As pointed out previously, porosity (of birds) has

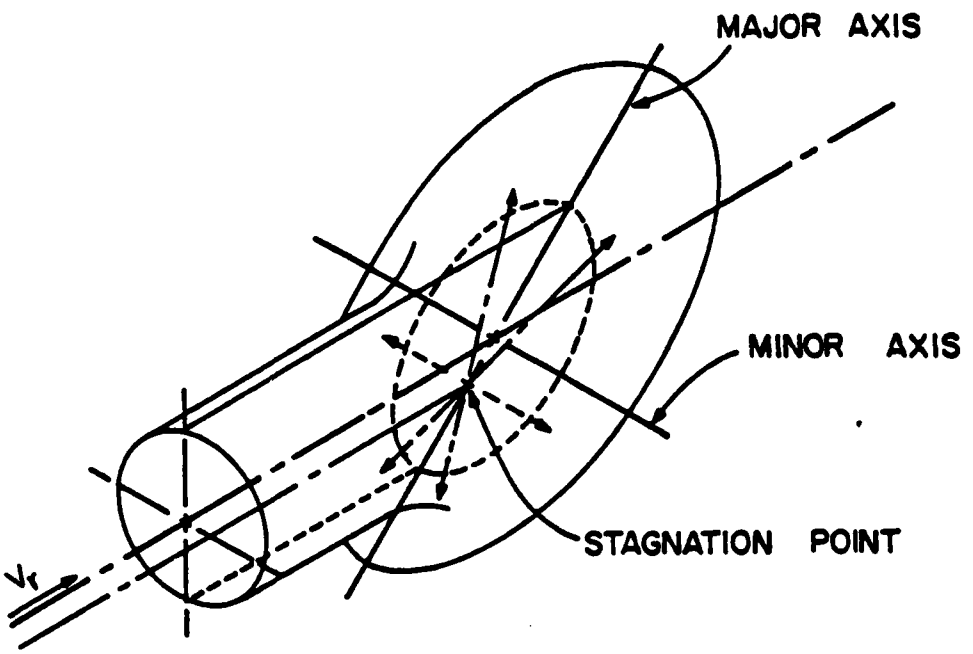

Figure 1. Oblique Impact

little effect on the stagnation pressure. The zero porosity density (ρ_f) and incompressible flow assumptions can, therefore, be applied. Thus, the problem is reduced to the classical hydrodynamic problem of the flow of a liquid jet onto a surface. The problem can be further simplified by making the assumption of irrotational flow: an assumption which is supported by the fact that in the impact region fluid inertia forces dominate over viscous forces. With the assumptions of steady, incompressible, irrotational flow, the problem may be treated as a steady, potential flow described by Laplace's equation. A serious complication remains however. The boundary of the jet is a free streamline whose position is not known "a priori." The static pressure is continuous across a free streamline while the velocity tangent to this streamline and the stagnation pressure are both discontinuous. Along a free streamline, the magnitude of the velocity is constant according to Bernoulli's equation. Thus, even though

the governing partial differential equation (Laplace's equation) is linear, the free streamline boundary condition is nonlinear. These conditions can be described, in two-dimensional flows, with complex variable theory and exact analytical solutions, and have been obtained, for two-dimensional jets impacting on flat surfaces. However, no three-dimensional jet impact flows (such as those of interest here) have been solved analytically. Not even the case of an axisymmetric (circular) jet impacting normal to a flat plate has been solved, because complex variable theory becomes extremely cumbersome in cylindrical coordinate systems.[6] Approximate analytical solutions are available for predicting the pressure distribution for circular jets impacting normal to flat plates.[1,7,8] Reference 8 contains semi-empirical expressions and techniques for computing pressure distributions for cylindrical jets impacting obliquely on flat surfaces. The general problem of a jet of an arbitrary cross section impacting on an arbitrary surface can only be solved by numerical methods.

Numerical potential flow solutions for jets (jets bounded by free streamlines) are very difficult to obtain because the location of the free streamlines are not, in general, known. For circular jets, at normal incidence, the position of the free streamlines can be adequately assumed in order to start a solution. For oblique impacts, particularly on curved surfaces, assuming the free streamline position would be a major undertaking in addition to the considerable task of numerically solving Laplace's equation in three dimensions. Accordingly, an approximate numerical solution which would provide a reasonably accurate description of the pressure distribution (but not necessarily satisfying the free streamline condition) was developed.

Three-dimensional potential flow theory was used to develop a model for predicting the pressure distribution produced by the steady flow of a cylindrical jet impacting on a flat plate. It was assumed that pressure distribution, as calculated for this fluid dynamic problem, would provide a reasonable description

of the steady flow portion of a bird impact. Incompressible, irrotational flow assumptions were made, but the free streamline boundary condition was not imposed. The method of superposition of solutions was used even though superposition is not strictly valid (although Laplace's equation is linear, the free stream boundary condition is nonlinear). The numerical approach used was based on the method of surface singularities.[4]

The approximate numerical solution involved the superposition of two elementary solutions to Laplace's equation. The two solutions used were: (1) the uniform flow of a fluid in an infinite jet of arbitrary but constant cross-sectional area; and (2) the uniform distribution of planar fluid sources over the impact area. The velocity of the fluid within the infinite jet was considered constant, while the fluid outside this region was assumed to be at rest. Surface sources were distributed on the target surface. The strength of the surface sources was selected to provide the correct boundary condition at the target (no flow normal to the target surface). The complete solution to this problem for jets of circular cross sections impacting obliquely on rigid flat surfaces was developed by Boehman of the University of Dayton and is presented in Reference 3.

This model can be used for any arbitrarily shaped impact surface. The impact area is divided into small flat elements, and a uniform distribution of sources is assumed to cover each element. During the analysis of an impact, in which local target deformation takes place, the deformed target shape in the impact zone is calculated at each time interval employed in the dynamic structural analysis. The geometry of the impact zone can then be provided at each time interval to the loading model, and the pressure distribution appropriate to the target at that time can be determined. As the structural analysis calculation proceeds, the local shape, location, and velocity of the impact area is updated and made available to the loading model. The loading model, in turn, provides updated pressure and pressure distribution

information for the structural response computation. The loading model is, thus, fully interactive with the structural response calculation. The duration of the impact is computed by computing the amount of slice consumed as a function of time and setting surface pressures equal to zero after the slice is consumed.

The loading model is capable of detailed interaction with the structural response model and is capable of dealing with target translation, rotation, and local deformation. The load/response coupling modelled in this formulation should be capable of accurate prediction of pressure for both overall target response and local deformation.

The principal limitation of the loading model is that it does not include transient effects. The most significant transient effect is the shock process. However, the porosity present in birds appreciably reduces the shock stresses, while the steady flow pressures are not significantly affected. In addition, impact obliquity (bird-blade impacts are, in general, oblique) also reduces the relative importance of shock stresses. Therefore, it is not obvious that neglect of the shock aspects of bird impact on blades is a significant deficiency. Another transient aspect of ice sphere impacts is the variation of a slice cross-sectional area at the target surface during impact. This results mainly in a time variation of the impact area. If the flow remains quasi-steady during these variations (i.e., the "velocity" of the variation is low with respect to local sound speed; probably a good assumption), then the model can be modified to describe these effects. The size and geometry of the "jet" which flows onto the target surface must be updated in time incrementally to describe the variation of impact area with time.

1.5 SUMMARY

In the current version of the loading model, the pressure distribution is based on a steady flow analysis. This method of analysis is extended into a dynamic analysis for deforming

targets by treating the flow at any instant of time as a quasi-steady flow using the instantaneous relative velocity between the bird slice and the deforming target as the characteristic velocity. The instantaneous shape of the target is used to define the surface on which impact occurs.

In the analysis of the impact process, the strength of the projectile material is considered to be negligible. This assumption is quite reasonable for the typical projectile and target materials of interest.

It is assumed that, at least as a first approximation, the fluid flow may be treated to be incompressible. This is a reasonable assumption in view of the fact that the measured steady-state pressures are quite small in comparison to the pressures required to produce significant density changes in birds or ice.[1]

By virtue of the incompressible flow and steady flow assumptions, together with negligible strength of the projectile material, the problem of predicting soft body impact loads is amenable to analysis within the following real constraints. The time required to obtain a reasonable solution must be small in comparison to the time required to compute the structural response, and the computer storage requirement for the loa ing model must be small in comparison to the structural analysis computer program storage requirements.

Three-dimensional potential flow theory was chosen as the most appropriate method for modelling the impact process. Our initial work in using this approach was quite successful.[3] In Reference 3, the method of surface singularities was used to determine the velocity and pressure fields due to circular jets impacting at oblique angles on flat rigid plates. This same technique was used to develop the loading model described in this report. The method developed in Reference 3 was generalized to include impact surface curvature and deformation velocity, arbitrary cross-sectional area of the impacting flow, and a method for generating planar quadrilateral surface elements given finite-element surface nodal point locations.

SECTION 2
DISCUSSION OF BIRD AND ICE IMPACT ON MOVING AND STATIONARY BLADES

While the discussion in the previous section dealt largely with the modeling of the soft-body impacts on surfaces (bird-strike on aircraft windshield, for example), the other area of major concern in the study of these impacts is the ingestion of foreign bodies in jet engines resulting in impacts on fan or compressor blading. Typically, this problem might arise from the ingestion of a bird or of ice sheets breaking off the nacelle. The primary consequences of such impact would be deflection, bending, and rupture of the impacted blades. Although this can give rise to secondary impacts and related effects, the present research program is confined only to the primary foreign object/blade impacts. It is useful to point out that while the subsequent discussion might explicitly deal with the bird/blade impact process, the analysis and the conclusions herein are not restricted to bird impact alone but apply to any foreign body impact (it is assumed, of course, that we would still be considering only "soft-body" materials).

The bird/blade impact process differs in an essential way from the earlier-discussed bird impact over extended surfaces. Unlike the bird striking an aircraft windshield, for instance, a bird entering an engine is cut into slices by the chopping action of the first-stage fan blades. Thus, before one proceeds with the analysis of the impact process, it is necessary to first establish the geometry and parameters of the slices of bird, or ice, formed by a rotating fan stage.

2.1 SLICING MODEL DEVELOPMENT

During 1976 a few experiments were conducted at the Air Force Materials Laboratory by the University of Dayton Research Institute to investigate the effects of slicing edge impacts on the impact loads. Birds were fired over thin wedges and

cylindrical wires mounted in a ballistic pendulum. From measurements of the momentum transfer during the slicing process, estimates of the slicing force could be made. It was found that the slicing force was predominantly due to fluid dynamic drag with no significant loading attributable to the cutting action itself. These experiments suggest that it is reasonable to ignore the cutting forces in comparison to the forces required to decelerate and/or change the direction of an impacting soft body. Therefore, the slicing model development reduces to simply a geometric problem of determining the dimensions and weight of a slice. For birds and ice spheres (such as hail) the velocity of the ingested object is small compared to the velocity of the aircraft; thus, the object velocity can be ignored. For ice slabs, such as ice breaking loose from an engine nacelle, the velocity of the slab relative to the nacelle is not well defined. A reasonable assumption, at least for short inlet systems, is to ignore the velocity of the slab relative to the nacelle. For long inlet systems, it might be possible to estimate the relative velocity between slab and nacelles by considering the action of aerodynamic drag forces on an ice slab after it has broken loose from a forward section of a nacelle.

2.1.1 Slicing Model Development for Birds

A bird is idealized as a right, circular cylinder with a length-to-diameter ratio of 2 and the velocity of the bird, relative to the aircraft, is taken to be equal and opposite to the aircraft velocity.

In the following analysis, a coordinate system attached to the blade is used. The bird/blade interaction geometry, in such a coordinate system, is shown in Figure 2. The following information is assumed to be known (supplied as input data to the loading model computer program):

N - number of blades per stage

n - blade rotational speed (rpm)

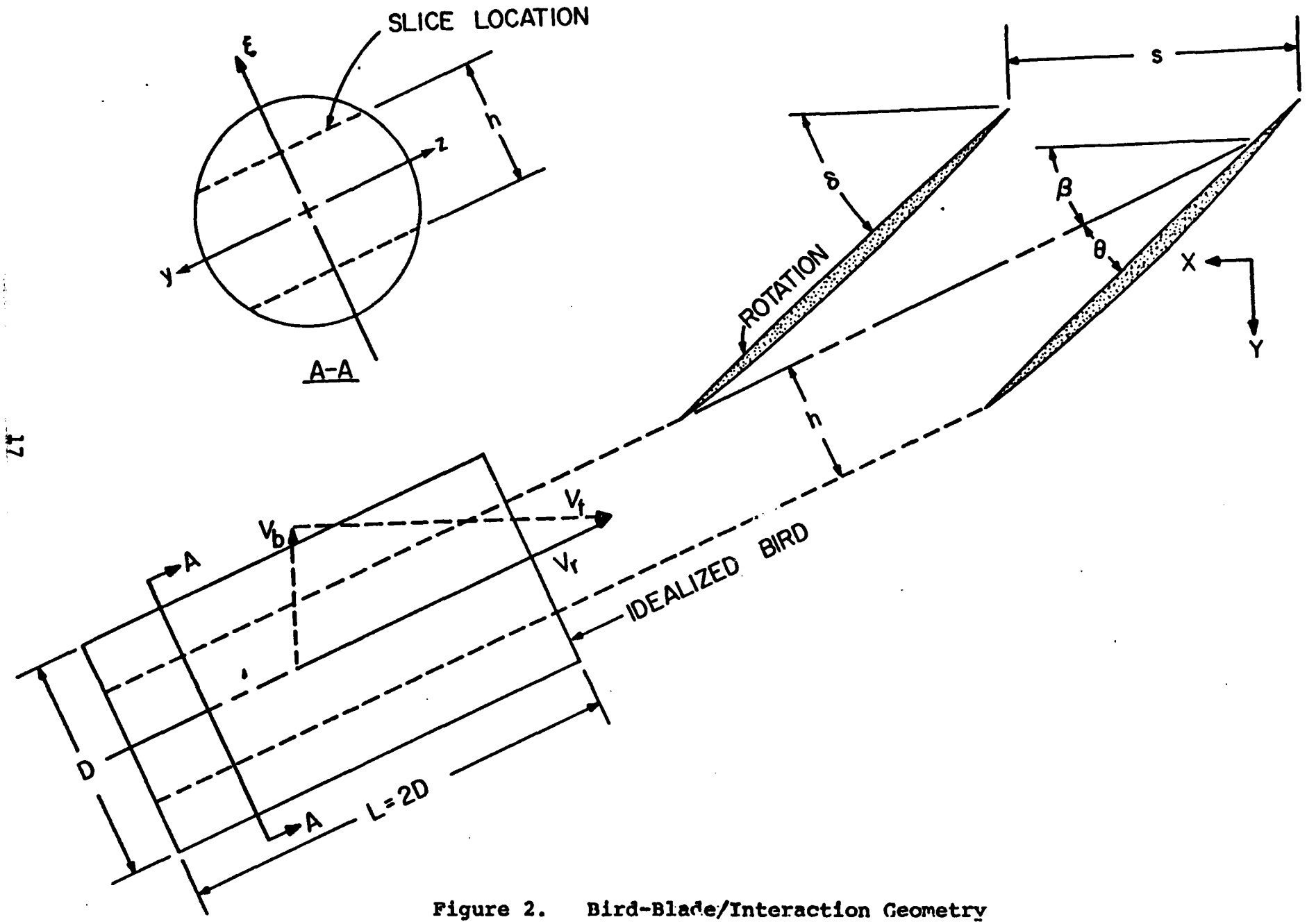

Figure 2. Bird-Blade/Interaction Geometry

Z_i - distance from the rotational axis of the rotor to the point on the blade at which the center of the impact occurs

δ - blade orientation angle (defined as the angle δ in Figure 1)

V_b - axial velocity of the bird

W_b - bird weight

ρ_b - bird density.

An infinite number of slice shapes is possible for a given set of these input parameters; the shape depends on the orientation of the bird relative to the blade, and on the span location on the blade at which the impact occurs. Since worst case slice shapes are desired (i.e., slice shapes having the largest possible slice mass), the orientation of the axis of the bird and the center of impact of a slice are chosen to produce a slice having the largest possible mass. The largest slice mass occurs when the axis of the slice is coincident with the axis of the right circular cylinder. The slice geometry depicted in Figure 2 corresponds to this worst case situation.

With the bird idealized as a right circular cylinder with L = 2D, the diameter of the bird is determined from the bird weight and density as

$$D = \left(\frac{2W_b}{\pi \rho_b}\right)^{1/3} \tag{1}$$

The tangential velocity of the bird V_t is computed at the impact radius Z_i and is given by

$$V_t = \frac{2\pi n Z_i}{60} \tag{2}$$

and the magnitude of the velocity of the bird relative to the blade V_r is given by

$$V_r = \sqrt{(V_b^2 + V_t^2)} \tag{3}$$

The direction of V_r relative to the plane of rotation of the blade β at the impact location Z_i is

$$\beta = \sin^{-1}(V_b/V_r) \quad . \tag{4}$$

V_r is assumed to have no component in the radial direction. The impact angle, defined as θ in Figure 2 is

$$\theta = \delta - \beta \tag{5}$$

and the blade spacing (defined as Z_i and denoted by S in Figure 2) is given by

$$S = 2\pi Z_i/N \quad . \tag{6}$$

The bird slice width, h, is then given by

$$h = S\sin\beta = \frac{2\pi Z_i}{N} \frac{V_b}{V_r} \tag{7}$$

Referring to Figure 2 we find that the bird-slice weight is given by

$$W_{s_b} = \rho_b L \int_{-h/2}^{+h/2} 2\sqrt{\left(\frac{D}{2}\right)^2 - \xi^2}\, d\xi$$

$$W_{s_b} = 2\rho_b D \left[h\sqrt{\left(\frac{D}{2}\right)^2 - \left(\frac{h}{2}\right)^2} + \frac{1}{2} D^2 \sin^{-1}\left(\frac{h}{D}\right)\right] \quad . \tag{8}$$

The use of Equations 2 and 3 in Equation 7 shows that the bird-slice width at any impact radius depends only on the blade parameters, N and n, and on the aircraft speed. The bird-slice weight at any impact radius depends, in addition to the above three parameters, only on the density and total weight of the bird.

If $h/\sin\theta$ is greater than the cord of the blade at Z_i, then not all of the slice will impact on the blade.

2.1.2 Slicing Model for Ice Spheres

For ice spheres (such as hail) the axial velocity of the sphere relative to the blade is taken to be equal and

opposite to the aircraft velocity, just as for birds. The same expressions for slice width impingement angle, and V_r, applies as for birds. The slice weight $W_{s_{is}}$ is given by

$$W_{s_{is}} = 2\pi\rho_i \int_0^{h/2} \left[\left(\frac{D}{2}\right)^2 - \xi^2\right] d\xi$$

or

$$W_{s_{is}} = 2\pi\rho_i \left[\left(\frac{D}{2}\right)^2\left(\frac{h}{2}\right) - \frac{1}{3}\left(\frac{h}{2}\right)^3\right] \qquad (9)$$

where $\frac{h}{2} \leq \frac{D}{2}$

and ρ_i is the ice density. For ice spheres it is presumed that the diameter of the sphere is a specified quantity along with the ice density.

2.1.3 Slicing Model for Ice Slab

For slabs of ice the operator specified information is presumed to be the length of the slab, L, the thickness of the slab, ΔZ, (i.e., how much of the blade span is to be exposed to the slab) and the axial velocity of the slab relative to the nacelle (this replaces V_b in Equations 3, 4, and 7). The slice width, h, is again given by Equation 7 with V_b replaced by the axial velocity of the slab relative to the nacelle. The slice mass is then given by

$$W_{s_s} = \rho_i(h)(\Delta Z)L \qquad (10)$$

2.2 BIRD SLICE GEOMETRY PARAMETRIC STUDY RESULTS

Using the equations developed in paragraph 2.1.2, the bird-slice parameters were computed for both starling impacts (3-ounce birds) and big bird impacts (1.5-pound birds). Three different blade configurations, viz., J-79, APSI, and F-101, are considered and typical values of the rotor speed, number of blades per stage, blade orientation angle, and impact radius are used. The input parameters and the computed quantities are shown for the two cases

of bird weights in Tables I and II. The primary observation from this parametric study is that bird (and ice sphere) impacts are highly oblique.

2.3 DURATION OF IMPACT

The amount of a slice consumed at any time during impact is directly related to the velocity of the slice relative to the blade (V_r in Figure 1).

TABLE I. BLADE CALCULATION INPUT DATA SHEET (3-OZ BIRD)

PARAMETER	J-79		APSI		F-101	
Rotor Speed, n (rmp)	7460		17500		7555	
No. of Blades, N	21		28		50	
Tip Radius, R_t (in.)	14.65		11.00		22.18	
Root Radius, R_R (in.)	5.21		4.95		11.71	
Span Location (%)	30	70	30	70	30	70
Radius, z_i (in.)	8.04	11.82	6.76	9.19	14.85	19.04
Orientation Angle, δ (°)	72.0	51.0	49.8	27.0	52.5	33.5
Chord Length, c (in.)	2.23	2.23	2.90	3.06	3.30	3.70
Calculated Values						
Blade Tangential Velocity, V_t (ft/s)	523	769	1032	1403	979	1255
Bird Axial Velocity, V_b (ft/s)	200	200	200	200	200	200
Relative Velocity, V_r (ft/s)	560	795	1051	1417	999	1270
Bird Weight, W_b (lb)	0.188	0.188	0.188	0.188	0.188	0.188
Bird Slice Width, h (in.)	0.86	0.89	0.29	0.29	0.37	0.38
Bird Slice Weight, W_s (lb)	0.126	0.129	0.045	0.045	0.057	0.058
Bird-Blade Incidence Angle, θ (°)	51.1	36.4	38.8	18.9	41.0	24.4
Angle β (°)	20.9	14.6	11.0	8.1	11.5	9.1
Bird Diameter, D (in.)	1.53	1.53	1.53	1.53	1.53	1.53

TABLE II. BLADE CALCULATION INPUT DATA SHEET (1.5-LB BIRD)

PARAMETER	J-79		APSI		P-101	
Rotor Speed, n (rmp)	7460		17500		7555	
No. of Blades, N	21		28		50	
Tip Radius, R_t (in.)	14.65		11.00		22.18	
Root Radius, R_R (in.)	5.21		4.95		11.71	
Span Location (%)	30	70	30	70	30	70
Radius, z_i (in.)	8.04	11.82	6.76	9.19	14.85	19.04
Orientation Angle, δ (°)	72.0	51.0	49.8	27.0	52.5	33.5
Chord Length, c (in.)	2.23	2.23	2.90	3.06	3.30	3.70
Calculated Values						
Blade Tangential Velocity, V_t (ft/s)	523	769	1032	1403	979	1255
Bird Axial Velocity, V_b (ft/s)	200	200	200	200	200	200
Relative Velocity, V_r (ft/s)	560	795	1051	1417	999	1270
Bird Weight, W_b (lb)	1.50	1.50	1.50	1.50	1.50	1.50
Bird Slice Width, h (in.)	0.86	0.89	0.29	0.29	0.37	0.38
Bird Slice Weight, W_s (lb)	0.53	0.55	0.18	0.18	0.23	0.24
Bird-Blade Incidence Angle, θ (°)	51.1	36.4	38.8	18.9	41.0	24.4
Angle β (°)	20.9	14.6	11.0	8.1	11.5	9.1
Bird Diameter, D (in.)	3.07	3.07	3.07	3.07	3.07	3.07

SECTION 3
POTENTIAL FLOW MODELING OF FOD IMPACTS

The impact of a soft body material (bird or ice slices) on a single blade is modelled using a well developed method of potential flow theory known as the surface singularity method. The procedure used to apply the method of surface singularities to FOD impact is based largely on the work of Hess and Smith.[4,9]

3.1 GENERAL DESCRIPTION OF THE SURFACE SINGULARITY METHOD

The method of surface singularities has its origin in a well-known theorem of potential flow theory which, in essence, states that if the velocity potential or its derivative is known over the entire boundary of a potential flow, then the velocity field may be determined throughout the region of the flow.[6] With this theorem, and with the aid of Green's theorem, Green's equivalent stratum of sources and doublets (singularities) is developed. This stratum essentially states that the velocity potential of a fluid in motion can be expressed in terms of either a distribution of sources and/or doublets over the flow boundary.[6] For nonlifting potential flows, only source distributions need be considered whereas doublet distributions are required for analysis of lifting potential flows.[10] Source distributions are considerably easier to implement and, based upon the good results obtained in our preliminary work using source distributions,[3] only source distributions are used in the model described in this report. The method of surface singularities as used in the FOD impact model utilizes a distribution of source density on the boundaries of the flow, and solves for the distribution of source density necessary to satisfy specified boundary conditions. Once the source density distribution is known, the flow velocities on the boundaries of the flow field and throughout the flow field can be computed.

In order to understand the method of surface singularities, consider a steady flow of a perfect fluid impinging on a three-dimensional body as shown in Figure 3. In the initial discussion

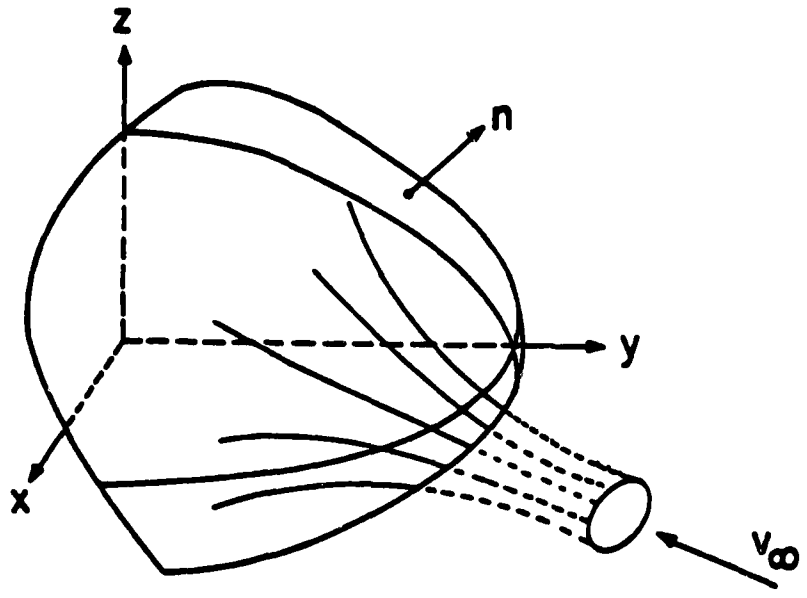

Figure 3. A Three-Dimensional Flow Field

of the method, the steady flow will be considered to be infinite in extent. The modifications required to adapt the method to flows of finite extent such as jet flows will be discussed later.

3.1.1 Surface Singularity for Flows of Infinite Extent

Let S be the surface of the body and have an equation of the form

$$F(x, y, z) = 0 \tag{11}$$

where x, y, and z are the Cartesian coordinates. For simplicity assume that the onset flow (defined as the flow field) is a uniform stream of unit magnitude, and let it be denoted by the constant vector $\vec{V}_\infty$ with components V_{∞_x}, V_{∞_y}, and V_{∞_z}, respectively, along the coordinates axes x, y, and z where;

$$V_\infty = \sqrt{V_{\infty_x}^2 + V_{\infty_y}^2 + V_{\infty_z}^2} = 1 \tag{12}$$

The fluid velocity at a point may be expressed as the negative gradient of a potential function ϕ. Which satisfies Laplace's Equation in the region R' exterior to the surface S, has a zero normal derivative on S, and approaches the proper uniform stream potential at infinity. Making use of the superposition principle, the potential function ϕ is viewed as

$$\phi = \phi_\infty + \phi \tag{13}$$

where ϕ_∞ is the uniform stream potential and is equal to

$$\phi_\infty = -(V_{\infty x}x + V_{\infty y}y + V_{\infty z}z) \tag{14}$$

and ϕ is the disturbance potential due to the body. Then ϕ should satisfy

$$\Delta\phi = 0 \quad \text{in } R' \tag{15}$$

$$\left.\frac{\partial\phi}{\partial n}\right|_S = \vec{n} \cdot \text{grad}\phi \Big|_{F=0} = \vec{n} \cdot \vec{V}_\infty \Big|_{F=0} \tag{16}$$

$$\phi \to 0 \quad \text{for } x^2 + y^2 + z^2 \to \rho_\infty \tag{17}$$

where Δ denotes the Laplacian operator and $\vec{n}$ is the unit outward normal vector at a point of the surface.

From potential theory, it can be shown that this potential may be evaluated in terms of a surface source density distribution with which the body surface may be considered to be covered.[6] Then ϕ may be written as

$$\phi(x,y,z) = \iint_S \frac{\sigma(q)}{r(p,q)}\, ds \tag{18}$$

where $r(p,q)$ is the distance from the integration point, q, on the surface to the field point, p, where the potential is being evaluated as shown in Figure 4. The function σ must be determined so that ϕ satisfies the normal derivative condition, Equation 16. On the body surface the normal derivative of ϕ is

$$\left.\frac{\partial\phi}{\partial n}\right|_S = -2\pi\sigma(p) + \iint_S \frac{\partial}{\partial n}\frac{1}{r(p,q)}\sigma(q)ds \ . \tag{19}$$

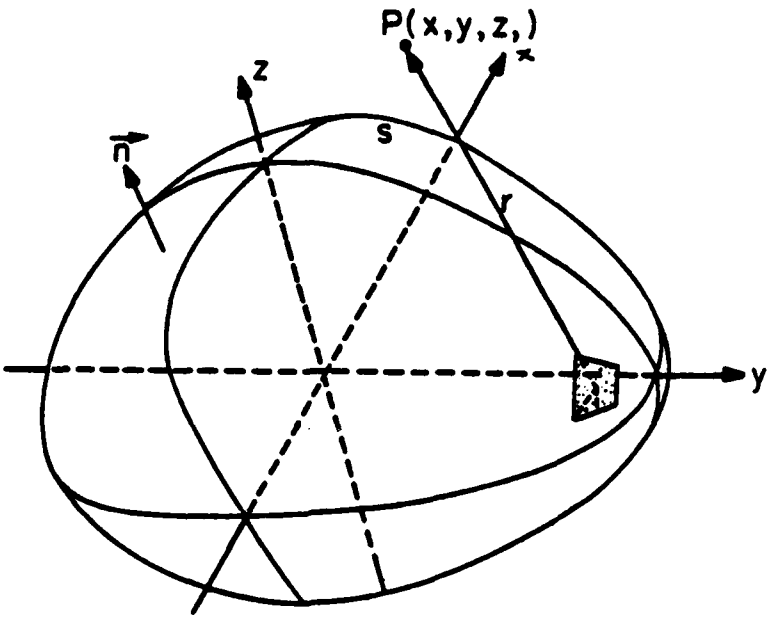

Figure 4. Notation used in Describing the Potential Due to a Surface Source Density Distribution

Substituting the value of $\frac{\partial \phi}{\partial n}\Big|_S$ in Equation 16 gives the integral equation for σ as

$$2\pi\sigma(p) - \iint_S \frac{\partial}{\partial n}\left(\frac{1}{r(p,q)}\right)\sigma(q)\,ds = \vec{n}(p)\cdot\vec{V}_\infty \qquad (20)$$

This is seen to be a two-dimensional Fredholm integral equation of the second kind over the surface, S. Once this equation is solved for σ, the disturbance potential ϕ may be evaluated from Equation 18 and the disturbance flow velocities from the derivatives of Equation 19 in the coordinate directions.

Some advantages of this method are: the equation that must be solved is a two-dimensional one over the body surface rather than a three-dimensional one over the entire exterior flow field, and the method can be used to calculate flows about arbitrary bodies. There is no restriction that the body be slender, analytic, or simply, connected or that the disturbance velocities due to the body be small compared with the velocity of the onset flow. However, it is required that the body surface have a continuous normal vector $\vec{n}$.

3.1.2 Complications of Flow of Finite Extent

For flows of finite extent, such as jet flows, obtaining an exact solution requires that the boundary streamlines of the flow must be included as part of the flow surface, S, over which sources are distributed. The addition of this surface poses severe complications. As was mentioned in paragraph 1.4, the position of the boundary streamline of the jet is unknown. Furthermore, the jet surface streamlines are a special type of streamline known as free streamlines along which the magnitudes of the velocity is constant. The difficulties which the presence of a free streamline causes in attempting to obtain exact numerical or analytical solutions were discussed in paragraph 1.4. Because of the very real computer time and computer storage limitations that had to be considered in the development of the present model, it was not feasible to attempt an exact numerical solution. Fortunately, reasonably accurate pressure distributions can be obtained with the surface singularity method without attempting to satisfy the free streamline boundary condition exactly. This is accomplished by use of a suitable model for the onset flow. Thus, in the FOD loading model discussed in this report, sources are distributed only over the surface on which the impact occurs. The model thus utilizes the same basic procedure as that described in paragraph 3.1.1 for flows of infinite extent, except that the onset flow velocity distribution is now not a constant velocity field but is a spatially varying velocity field. As is shown in Reference 3, even the simplest possible onset flow model, which has a uniform distribution of velocity over the cross sectional area of the impacting object and zero velocity everywhere else, gives surprisingly good results.

3.2 DETAILED DESCRIPTION OF THE COMPUTATIONAL PROGRAM

In this section, a detailed description of the computer program used to solve for the source density distribution, the disturbance potential, and the disturbance flow velocities along with their analytical equations are presented.

3.2.1 The Body Surface Approximation

To allow arbitrary bodies to be considered, it is required that the body surface be specified by a set of points in space called input points. Then the body surface is approximated by a large number of small plane quadrilateral elements. These elements are formed from the original points defining the body surface as shown in Figure 5.

In the original application of the surface singularity method to FOD impacts[3], rectangular surface elements were used. However, in the development of that model no attempt was made to interface it with a finite element structural analysis program, and the impact surface was flat and assumed to be rigid. Thus, rectangular elements were preferred due to their computational simplicity. In that model, the coordinates of the center of each element, and the lengths of the long and short sides, were read in as input data. The present model is designed specifically to be interfaced with finite element structural analysis computer

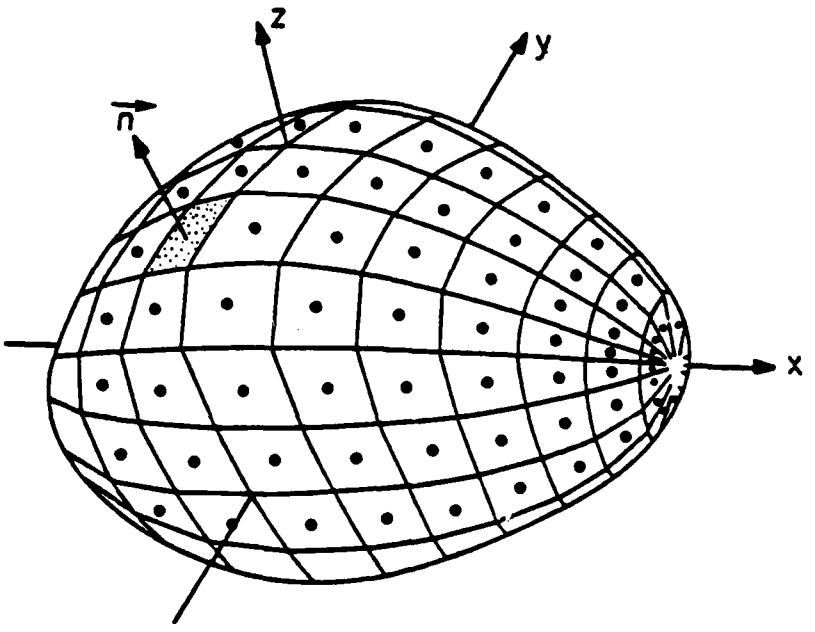

Figure 5. The Approximate Representation of the Body Surface

programs and is designed to handle impacts on arbitrarily curved surfaces. Quadrilateral elements provide a better approximation to an arbitrarily curved surface than rectangular elements and are much easier to construct from the finite element representation of a curved surface. In the model, it is required that the coordinates of all nodal points on the impacted surface be supplied to the loading model. Specifically, the nodal points in the finite-element program become approximate locations of the null point (defined to be the point where the quadrilateral element induces no velocity in its own plane) around which the plane quadrilateral elements are constructed in the potential flow analysis. This greatly facilitates the coupling of the finite-difference loading model and the finite-element structural code. Null points are the points at which, with the least amount of computational effort and with the greatest accuracy, the surface pressures can be computed in the loading model. The surface nodal locations are the points where the finite element structural code requires the surface loads to be defined.

Input to the loading model consists of the coordinates of the set of finite element nodal points defining the surface of the impacted object. These coordinates are given in the reference coordinate system, that is, the coordinate system used to describe the shape of the impacted surface before impact occurs. Each nodal point is identified by a pair of integers, m and n, where n identifies the column of points to which it belongs and m defines its position in the column. For a fan blade analysis the undeformed blade is imagined first to be cut into (NS-1) strips by NS cuts (n-lines) proceeding from root to tip with these cuts orientated basically along chord lines. Then the blade is cut into (NC-1) strips by NC cuts (m-lines) proceeding from the leading edge to trailing edge. The integer n thus ranges from 1 to NS, and the integer m ranges from 1 to NC. The intersections of these cuts define the initial position of the surface nodal points (before impact).

Quadrilateral elements are computed from groups of four neighboring nodal points which, for nonflat surfaces, do not generally lie in a plane. Consider a nodal point identified by (m,n) which is not on the first or last m or n lines (boundary lines). Nodal points lying on boundary lines require special treatment which is discussed later in this section. The first step in defining a quadrilateral is to locate four points around the nodal point (m,n) which can be thought of as "corner" points for a surface with four edges but which, in general, will not be a plane quadrilateral. These four "corner" points are located midway along each of four vectors connecting the nodal point (m,n) with nodal points (m-1,n-1), (m+1,n-1), (m+1,n+1), and (m-1,n+1). These points are labeled 1, 2, 3, and 4 respectively as shown in Figure 6 and will hereafter be called mid-node points. The coordinates of the mid-node points are:

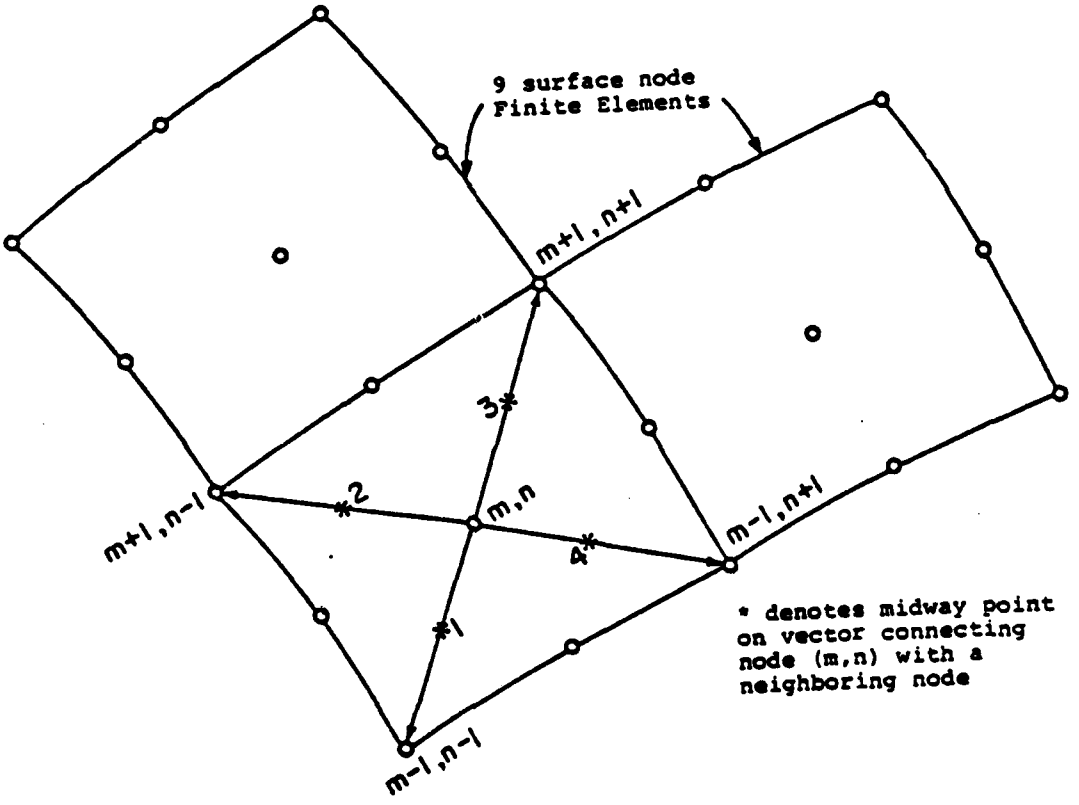

Figure 6. Nodal Numbering System and Mid-Node Point Formulation And Numbering

$$1: \quad X_1, \; Y_1, \; Z_1$$
$$2: \quad X_2, \; Y_2, \; Z_2$$
$$3: \quad X_3, \; Y_3, \; Z_3$$
$$4: \quad X_4, \; Y_4, \; Z_4$$

It should be noted that once a mid-node point is defined for one element, it can be used in the formation of up to three neighboring elements. Therefore, it is not necessary to actually construct all four vectors shown in Figure 6 for each nodal point.

Nodal points lying on boundary lines obviously do not have four neighboring nodal points. For nodal points on the leading edge of the blade (m=1), the node point is not used as the null point. For these points mid-node points 1 and 4 corresponding to node point (2,n) are used to define mid-node points 2 and 3 for the (1,n) leading edge node point. "Corner" points 1 and 4 are defined by projecting half the distance to neighboring leading edge node points if they exist. If they do not exist [nodes (1,1) and (1,NS)], then they are artificially generated by projecting off the blade along the leading edge by a distance equal to one-half the distance to the leading edge neighbor which does exist.

Mid-node points for nodes lying on the other three boundary lines are formed from those mid-node points which they share with other nodal points. Any missing "corner" points are formed by projecting off the surface of the blade by an amount which does not exceed one half the distance to its nearest neighboring nodal points.

3.2.2 Formation of the Plane Quadrilateral Surface Element

The plane quadrilateral surface elements are formed from the four appropriate mid-node points as follows. First the two "diagonal" vectors $\vec{T}_1$ and $\vec{T}_2$ are formed (Figure 7). Vector $\vec{T}_1$ goes from 1 to 3 and vector $\vec{T}_2$ goes from 2 to 4. In general, these vectors are not orthogonal and do not intersect. Their components are:

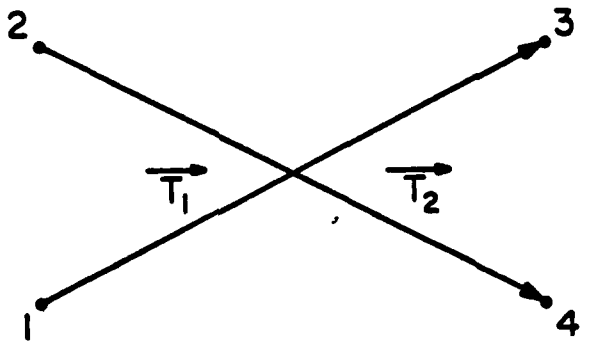

Figure 7. Formation of an Element From Four Mid-Node Points

$$\begin{aligned} T_{1x} &= X_3 - X_1 \quad T_{1y} = Y_3 - Y_1 \quad T_{1z} = Z_3 - Z_1 \\ T_{2x} &= X_4 - X_2 \quad T_{2y} = Y_4 - Y_2 \quad T_{2z} = Z_4 - Z_2 \end{aligned} \tag{21}$$

The cross product, $\vec{N}$, of these vectors divided by its own length is taken as the unit normal vector, $\vec{n}$, to the plane of the element.

$$\vec{N} = \vec{T}_2 \times \vec{T}_1 \tag{22}$$

The components of $\vec{N}$ are:

$$\begin{aligned} N_x &= T_{2y}T_{1z} - T_{1y}T_{2z} \\ N_y &= T_{1x}T_{2z} - T_{2x}T_{1z} \\ N_z &= T_{2x}T_{1y} - T_{1x}T_{2y} \end{aligned} \tag{23}$$

The components of the unit normal vector $\vec{n}$ are:

$$\begin{aligned} n_x &= \frac{N_x}{N} \\ n_y &= \frac{N_y}{N} \\ n_z &= \frac{N_z}{N} \end{aligned} \tag{24}$$

where $$N = \sqrt{N_x^2 + N_y^2 + N_z^2} \tag{25}$$

To completely specify the plane of the element a point in the plane is also required. This point is taken as the point whose coordinates $\bar{X}$, $\bar{Y}$, $\bar{Z}$ are the averages of the coordinates of the four mid-node points, i.e.,

$$\begin{aligned} \bar{X} &= \tfrac{1}{4}(X_1 + X_2 + X_3 + X_4) \\ \bar{Y} &= \tfrac{1}{4}(Y_1 + Y_2 + Y_3 + Y_4) \\ \bar{Z} &= \tfrac{1}{4}(Z_1 + Z_2 + Z_3 + Z_4) \end{aligned} \tag{26}$$

Now the mid-node points will be projected into the plane of the element along the normal vector. The resulting points are the corner points of the plane quadrilateral source element and these, rather than the mid-node points, are the points used in all calculations. The signed distance of the k-th mid-node point (k=1,2,3,4) from the plane is

$$d_k = n_x(\bar{X} - X_k) + n_y(\bar{Y} - Y_k) + n_z(\bar{Z} - Z_k) \tag{27}$$

and the coordinates of the corner points in the reference coordinate system are given by

$$\begin{aligned} X_k' &= X_k + n_x d_k \\ Y_k' &= Y_k + n_y d_k \\ Z_k' &= Z_k + n_z d_k \end{aligned} \tag{28}$$

3.2.3 Formation of the Element Coordinate System

It is convenient to derive and to use the formulas for the velocities induced by a quadrilateral source element of uniform strength at points in space assuming the element to lie in a coordinate plane. This necessitates constructing a coordinate system having two of its axes in the plane of the element. Thus, three mutually perpendicular unit vectors are required, two of which are in the plane of the element and one of which is normal to it.

The unit normal vector is taken as one of the unit vectors, and the unit vectors in the plane of the element are denoted by $\vec{t}_1$ and $\vec{t}_2$. $\vec{t}_1$ is taken as $\vec{T}_1$ divided by its own length, i.e.,

$$t_{1x} = \frac{T_{1x}}{T_1}$$
$$t_{1y} = \frac{T_{1y}}{T_1} \qquad (29)$$
$$t_{1z} = \frac{T_{1z}}{T_1}$$

where

$$T_1 = \sqrt{T_{1x}^2 + T_{1y}^2 + T_{1z}^2} \qquad (30)$$

The vector $\vec{t}_2$ is defined by $\vec{t}_2 = \vec{n} \times \vec{t}_1$, so that its components are:

$$t_{2x} = n_y t_{1z} - n_z t_{1y}$$
$$t_{2y} = n_z t_{1x} - n_x t_{1z} \qquad (31)$$
$$t_{2z} = n_x t_{1y} - n_y t_{1x}$$

To transform the coordinates of points and the components of vectors between the reference coordinate system and the element coordinate system, the transformation matrix is required.

The elements of this matrix are the components of the three basic unit vectors, $\vec{t}_1$, $\vec{t}_2$, $\vec{n}$.

The transformation matrix is thus the array

$$\begin{array}{lll} a_{11} = t_{1x} & a_{12} = t_{1y} & a_{13} = t_{1z} \\ a_{21} = t_{2x} & a_{22} = t_{2y} & a_{23} = t_{2z} \\ a_{31} = n_x & a_{32} = n_y & a_{33} = n_z \end{array} \qquad (32)$$

To transform the coordinates of points from one system to the other, the coordinates of the origin of the element coordinate system in the reference coordinate system are

required; let these be denoted X_o, Y_o, Z_o. Then, if a point has coordinates X', Y', Z' in the reference coordinate system and coordinates X, Y, Z in the element coordinate system, the transformation from the reference to the element system is

$$\begin{aligned} X &= a_{11}(X'-X_o) + a_{12}(Y'-Y_o) + a_{13}(Z'-Z_o) \\ Y &= a_{21}(X'-X_o) + a_{22}(Y'-Y_o) + a_{23}(Z'-Z_o) \\ Z &= a_{31}(X'-X_o) + a_{32}(Y'-Y_o) + a_{33}(Z'-Z_o) \end{aligned} \tag{33}$$

while the transformation from the element to the reference system is

$$\begin{aligned} X' &= X_o + a_{11}X + a_{21}Y + a_{31}Z \\ Y' &= Y_o + a_{12}X + a_{22}Y + a_{32}Z \\ Z' &= Z_o + a_{13}X + a_{23}Y + a_{33}Z \end{aligned} \tag{34}$$

The origin is temporarily taken as the point whose coordinates are the averages of the four mid-node points, i.e., the point with coordinates $\overline{X}$, $\overline{Y}$, $\overline{Z}$ in the reference system , and is used to find the coordinates of the centroid of the area (Figure 8).

The corner points are transformed into the element coordinate system based on the average point as origin. Their coordinates in the element coordinate system are denote by ξ_k^*, η_k^*, 0. Because they lie in the plane of the element, they have a zero ζ coordinate in the element coordinate system. Using the above transformation these coordinates are:

$$\begin{aligned} \xi_k^* &= a_{11}(X_k-\overline{X}) + a_{12}(Y_k-\overline{Y}) + a_{13}(Z_k-\overline{Z}) \\ \eta k^* &= a_{21}(X_k-\overline{X}) + a_{22}(Y_k-\overline{Y}) + a_{23}(Z_k-\overline{Z}) \end{aligned} \tag{35}$$

The origin of the element coordinate system is now transferred to the centroid of the area of the quadrilateral. With the average point as origin, the coordinates of the centroid in the element coordinate system are:[4]

$$\xi_o = \frac{1}{3}\frac{I}{\eta_2^*-\eta_4^*}\left[\xi_4^*(\eta_1^*-\eta_2^*) + \xi_2^*(\eta_4^*-\eta_1^*)\right] \tag{36}$$

$$\eta_o = -\frac{1}{3}\eta_1^*$$

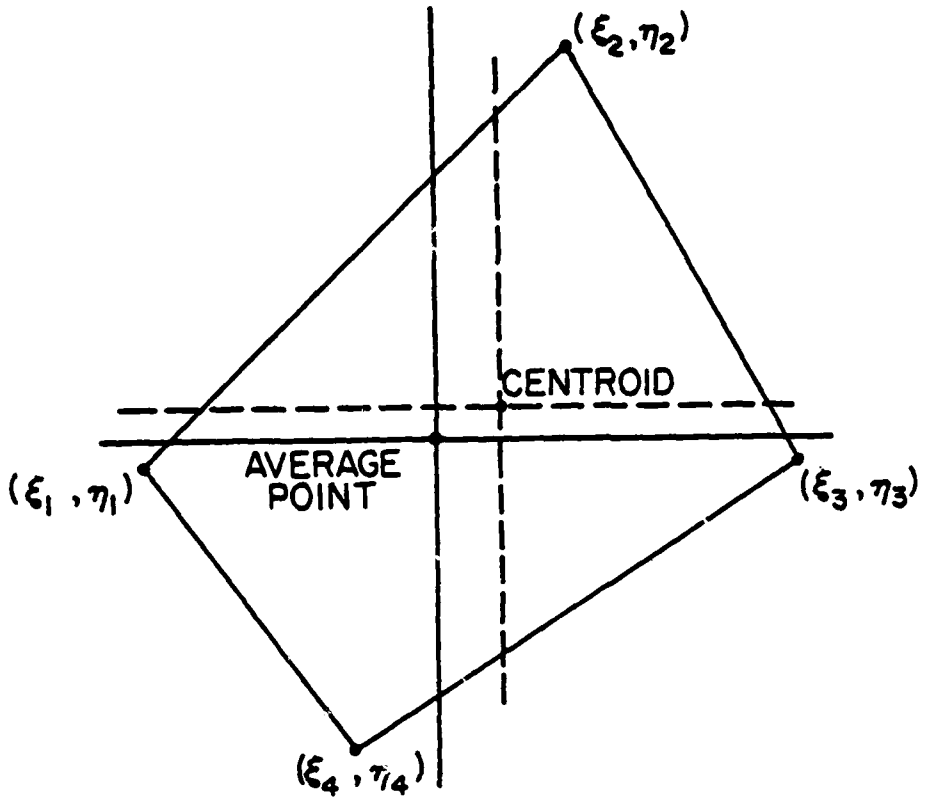

Figure 8. A Plane Quadrilateral Element, Transfer of Origin from Average Point to the Centroid

These are subtracted from the coordinates of the corner points in the element coordinate system based on the average point as origin to obtain the coordinates of the corner points in the element coordinate system based on the centroid or origin, i.e.,

$$\begin{aligned} \xi_k &= \xi_k^* - \xi_o \\ \eta_k &= \eta_k^* - \eta_o \end{aligned} \qquad k = 1,2,3,4 \tag{37}$$

Since the centroid is to be used as the origin of the element coordinate system, its coordinates in the reference coordinate system are required for use with the transformation matrix. These coordinates are:

$$\begin{aligned} X_o &= \bar{X} + a_{11}\xi_o + a_{21}\eta_o \\ Y_o &= \bar{Y} + a_{12}\xi_o + a_{22}\eta_o \\ Z_o &= \bar{Z} + a_{13}\xi_o + a_{23}\eta_o \end{aligned} \tag{38}$$

3.2.4 Determination of Null Point

It is necessary to select a particular point on each quadrilateral element where the normal velocity will be required to vanish and where the flow velocities will be computed. This point is taken as the point where the quadrilateral induces no velocity in its own plane. It is designated the null point. The x and y coordinates of this point, in the element coordinate system, are obtained as the solution of two simultaneous, non-linear equations. These equations are

$$\begin{aligned} V_x(X,Y) &= 0 \\ V_y(X,Y) &= 0 \end{aligned} \tag{39}$$

where V_x and V_y are the velocity components induced by a quadrilateral source element of unit source density. They are derived from the fundamental potential function. The general equations of the induced velocity components are:[4]

$$\begin{aligned} V_x = {} & \frac{\eta_2-\eta_1}{d_{12}}\log\left(\frac{r_1+r_2-d_{12}}{r_1+r_2+d_{12}}\right) + \frac{\eta_3-\eta_2}{d_{23}}\log\left(\frac{r_2+r_3-d_{23}}{r_2+r_3+d_{23}}\right) \\ & + \frac{\eta_4-\eta_3}{d_{34}}\log\left(\frac{r_3+r_4-d_{34}}{r_3+r_4+d_{34}}\right) + \frac{\eta_1-\eta_4}{d_{41}}\log\left(\frac{r_4+r_1-d_{41}}{r_4+r_1+d_{41}}\right) \end{aligned} \tag{40}$$

$$\begin{aligned} V_y = {} & \frac{\xi_1-\xi_2}{d_{12}}\log\left(\frac{r_1+r_2-d_{12}}{r_1+r_2+d_{12}}\right) + \frac{\xi_2-\xi_3}{d_{23}}\log\left(\frac{r_2+r_3-d_{23}}{r_2+r_3+d_{23}}\right) \\ & + \frac{\xi_3-\xi_4}{d_{34}}\log\left(\frac{r_3+r_4-d_{34}}{r_3+r_4+d_{34}}\right) + \frac{\xi_4-\xi_1}{d_{41}}\log\left(\frac{r_4+r_1-d_{41}}{r_4+r_1+d_{41}}\right) \end{aligned} \tag{41}$$

$$\begin{aligned} V_z = {} & \tan^{-1}\left(\frac{m_{12}e_1-h_1}{zr_1}\right) - \tan^{-1}\left(\frac{m_{12}e_2-h_2}{zr_2}\right) \\ & + \tan^{-1}\left(\frac{m_{23}e_2-h_2}{zr_2}\right) - \tan^{-1}\left(\frac{m_{23}e_3-h_3}{zr_3}\right) \\ & + \tan^{-1}\left(\frac{m_{34}e_3-h_3}{zr_3}\right) - \tan^{-1}\left(\frac{m_{34}e_4-h_4}{zr_4}\right) \\ & + \tan^{-1}\left(\frac{m_{41}e_4-h_4}{zr_4}\right) - \tan^{-1}\left(\frac{m_{41}e_1-h_1}{zr_1}\right) \end{aligned} \tag{42}$$

where

$$d_{12} = \sqrt{(\xi_2 - \xi_1)^2 + (\eta_2 - \eta_1)^2}$$

$$d_{23} = \sqrt{(\xi_3 - \xi_2)^2 + (\eta_3 - \eta_2)^2} \qquad (43)$$

$$d_{34} = \sqrt{(\xi_4 - \xi_3)^2 + (\eta_4 - \eta_3)^2}$$

$$d_{41} = \sqrt{(\xi_1 - \xi_4)^2 + (\eta_1 - \eta_4)^2}$$

where

$$m_{12} = \frac{\eta_2 - \eta_1}{\xi_2 - \xi_1} \qquad m_{23} = \frac{\eta_3 - \eta_2}{\xi_3 - \xi_2}$$

$$m_{34} = \frac{\eta_4 - \eta_3}{\xi_4 - \xi_3} \qquad m_{41} = \frac{\eta_1 - \eta_4}{\xi_1 - \xi_4} \qquad (44)$$

and

$$r_k = \sqrt{(X - \xi_k)^2 + (Y - \eta_k)^2 + Z^2} \qquad k=1,2,3,4 \qquad (45)$$

and

$$e_k = Z^2 + (X - \xi_k)^2 \qquad k=1,2,3,4 \qquad (46)$$

$$h_k = (Y - \eta_k)(X - \xi_k) \qquad k=1,2,3,4 \qquad (47)$$

with $Z = 0$ and ξ_k, η_k set equal to the coordinates of the corner points, which were obtained in the previous section, these equations are solved by means of an iterative procedure, which utilizes analytic expression for the derivatives of V_x and V_y. With the notation $(\ )_x = \partial/\partial_x$, $(\ )_y = \partial/\partial_y$, the iterative procedure is as follows. Let X_p and Y_p denote the p-th approximation to the X and Y coordinates of the null point and let the notation $[\ ]^{(p)}$ denote the quantity in brackets evaluated at $X = X_p$, $Y = Y_p$. Once the p-th approximation has been found, the (p+1)-th approximation is obtained by solving the following pair of linear algebraic equations for X_{p+1}, Y_{p+1}.

$$[(V_x)_x]^{(p)}(X_{p+1} - X_p) + [(V_x)_y]^{(p)}(Y_{p+1} - Y_p) = -[V_x](p)$$

$$[(V_y)_x]^{(p)}(X_{p+1} - X_p) + [(V_y)_y]^{(p)}(Y_{p+1} - Y_p) = -[V_y](p) \qquad (48)$$

The first approximation is X = Y = 0. The iterative procedure is terminated when the induced velocity components at the approximate null point are both less in absolute value than a prescribed value. This value is set at 0.001.

3.2.5 Formation of the Vector Matrix of Influence Coefficients

The velocities induced by the quadrilateral source elements at each other's null points must be computed. This is done under the assumption that the source density on each element is of unit strength. The final result of this calculation is the complete set of the velocities induced at each null point by every quadrilateral element. This array may be thought of as a "matrix of influence coefficients," the elements of which are vectors in three-dimensional space.

The basic caluclation is the computation of the velocity components induced at the null point of the i-th element by a unit source density distribution on the j-th element.

The coordinates of the i-th null point X_{np}', Y_{np}', Z_{np}' are transformed into the j-th element coordinate system obtaining X_{np}, Y_{np}, Z_{np}. The transformation is accomplished by means of Equation 33. The velocity components are evaluated from Equations 40, 41, and 42. In these formulas X, Y, Z are replaced by X_{np}, Y_{np}, Z_{np} and ξ_k, η_k are the coordinates of the corner points of the j-th element.

In evaluating these velocity components, V_x and V_y cause no trouble. The component V_z requires special handling in certain cases. As $Z_{np} \to 0$, $V_z \to 0$ if the null point is approaching a point in the plane outside the boundaries of the quadrilateral. However, $V_z \to 2\pi(\text{Sign } Z_{np})$ if the null point is approaching a point within the quadrilateral.

Due to round off error which occurs while making the transformation from reference to element coordinate system, Z_{np} may have small values with either sign and the calculation of

V_z will give a value different than what it should be (i.e., 0 or 2π). To avoid this error, the absolute value of z_{np} is tested before velocities are computed and, if it is less than some small prescribed number (in this case it is the smaller diagonal/100), which is, nevertheless, large compared to the expected round-off error, z_{np} is set equal to zero and V_z is set equal to zero for points outside the quadrilateral or equal to $+2\pi$ for points inside the quadrilateral. Another situation that may cause trouble occurs when the slope of a side of the quadrilateral is infinite. To avoid difficulties each of the quantities $(\xi_2-\xi_1)$, $(\xi_3-\xi_2)$, $(\xi_4-\xi_3)$, and $(\xi_1-\xi_4)$ are tested to determine whether they are zero, and if any one of them is zero, the two inverse tangents corresponding to that side are set equal to zero. It should be mentioned that the inverse tangents in Equation 42 are evaluated in the normal range $-\pi/2$ to $+\pi/2$.

The induced velocity components V_x, V_y, V_z are in the element coordinate system and must be transformed to obtain the components V_x', V_y', V_z' in the reference coordinate system. This is done by using Equation 33 where V_x, V_y, V_z replace X, Y, Z, respectively, in these equations, and V_x', V_y', V_z' replace $(X'-X_o)$, $(Y'-Y_o)$, $(Z'-Z_o)$.

To obtain a set of linear lgebraic equations for the unknown values of the source density on the elements, the first step is to calculate the normal velocities induced at each null point by the various elements, each of which is still assumed to have a unit source density.

The normal velocity induced at the null point of the i-th element by a unit source density on the j-th element is obtained by taking the dot product of $\overrightarrow{V_{ij}}$ with the unit normal vector of the i-th element $\overrightarrow{n_i}$. $\overrightarrow{V_{ij}}$ is defined as the vector velocity induced at the null point of the i-th element by a unit source density on the j-th element. This induced normal velocity is denoted A_{ij}. It is given by

$$A_{ij} = \overrightarrow{V_{ij}} \cdot \overrightarrow{n_i} = n_{ix}V_x' + n_{ij}V_y' + n_{iz}V_z' \quad . \qquad (49)$$

The result is a scalar matrix whose elements are the normal velocities induced at the various null points by the various quadrilateral elements with unit source density. This matrix is the coefficient matrix of the required set of linear equations, since multiplying this by the column matrix of the unknown values of the source density on each element gives a column matrix whose elements are the true normal velocities induced at the null points by the entire approximate body surface. The right hand sides of the linear equations are the negatives of the normal components of the onset flow at the various null points.

3.2.6 Designation of the Onset Flow

The onset flow is used to form a right hand side for use with the coefficient matrix. The onset flow is designated by the vector $\overrightarrow{V_{\infty i}}$ and must be defined at each null point i. This vector will be a spatially varying function for flows of finite extent. It also varies with time for a deforming surface. Presently, the loading model uses the simple onset flow model described in paragraph 3.1.2 modified to include the effect of the displacement velocity of the deforming blade. The components of onset flow relative to the blade are given by

$$\begin{aligned} V_{\infty x} &= V_t + U_x \\ V_{\infty y} &= V_b + U_y \\ V_{\infty z} &= U_z \end{aligned} \qquad (50)$$

for all null points which lie under the projected area of the impacting object on the blade. The onset flow is specified as zero for all other null points. The onset flow velocity components, given by Equation 50, are defined in the reference coordinate system. For a blade analysis, the following reference coordinate system is used.

The positive X direction is in the direction of rotation of the rotor, the positive y direction is looking forward along the axis of the engine, and the Z direction is in the plane of rotation of the rotor with positive Z going from root to tip. The X, Y, and Z directions are shown in Figure 2. In Equation 50, U_x, U_y, and U_z represent the local deformation

velocity components of the blade and are supplied to the loading model by the structural analysis program.

More sophisticated onset flow models have been developed but have not as yet been incorporated into the loading model. These more sophisticated onset flow models attempt to take account the spreading of the jet as the impact surface is approached and, thereby, give a better description of the pressure distribution at the edges of the impact area. In Section 4, a more sophisticated onset flow model is presented which is based on two-dimensional jet theory.

3.2.7 The Linear Algebraic Equations for the Values of the Surface Source Density

3.2.7.1 Formulation of the Equations

Now the values of the surface source density on the elements will be obtained as the solution of a set of linear algebraic equations. Recall that the source density is assumed constant on each quadrilateral element. Thus, there are N unknown values of the source density, where N is the number of elements formed from the input point. The total normal velocity is required to vanish at the null point of each element formed from the nodal points; therefore, there are N equations for the N unknown values of the source density. The total velocity induced at the i-th null point by all quadrilateral elements is

$$N_i = \sum_{j=1}^{N} A_{ij}\sigma_j \qquad (51)$$

The normal component of the onset flow at the i-th null point is the dot product of the onset flow vector and the unit normal vector of the i-th element, i.e.,

$$V_{\infty ni} = \vec{n_i} \cdot \vec{V_\infty} = n_{ix}V_{\infty x} + n_{iy}V_{\infty y} + n_{iz}V_{\infty z} \qquad (52)$$

The total normal velocity at the i-th null point is the sum of Equations 51 and 52. Thus the requirement that the normal velocity vanish at all null points gives the following set of linear equations for the values of the source density

$$\sum_{j=1}^{N} A_{ij} \sigma_j = -V_{\infty ni} \qquad (53)$$

By solving this set of equations a complete set of source densities is obtained for this onset flow.

3.2.7.2 Solution of the Equations

If the impacted surface is perfectly flat, all of the off-diagonal members of A_{ij} are identically zero and the solution of A_{ij} is trivial;[3] no matrix operations are involved. For surfaces which are highly curved, the off-diagonal elements are generally small compared to the diagonal elements and matrix iterative solution procedures such as the Seidel procedure[4] must be used. This procedure gives good convergence and requires less computer time than direct elimination methods particularly when more than 200 elements are used. The Seidel procedure did not prove to be a very good method, however, for blade analysis. Difficulties with convergence were experienced with blade surfaces which were nearly flat before impact but which became slightly deformed and concave during the early stages of impact. In this situation many of the off-diagonal elements are of the same order of magnitude as diagonal elements and are not all of the same sign. Also, because of program storage limitations imposed on the loading model, it was not feasible to consider more than 80 to 100 elements. Therefore, a direct elimination method of solution is used to solve the equations. The method used is Gaussian elimination with pivotal condensation. A subroutine called CSOLVR, which was developed by one of the authors (Boehman), is used in the loading model computer program. This subroutine was originally developed to solve difficult linear systems such as those encountered in laminar, compressible boundary layer stability theory, and in large systems of chemical equilibrium reaction equations solved by the Newton-Raphson search procedure.

3.2.8 Calculation of Total Flow Velocities and Pressures

Once the values of the surface source density have been found, the actual flow velocities at the null points are

calculated by multiplying the elements of the "matrices of influence coefficients," which are the induced velocity components that were calculated assuming a unit value for all source densities, by the corresponding true values of the source densities, and summing all such products that are appropriate for the null point in question. To the results of this summation must be added the proper components of the onset flow. Recall that the velocity induced at the null point of the i-th element by a unit source density on the j-th element is the vector $\vec{V}_{ij}$ with components X_{ij}, Y_{ij}, Z_{ij} corresponding, respectively, to V_x', V_y', V_z'. Let the total flow velocity at the null point of the i-th element be denoted by the vector $\vec{V}_i$ with components V_{ix}, V_{iy}, V_{iz}. These components are given by

$$V_{ix} = \sum_{j=1}^{N} X_{ij}\sigma_j + V_{\infty x}$$

$$V_{iy} = \sum_{j=1}^{N} Y_{ij}\sigma_j + V_{\infty y} \qquad (54)$$

$$V_{iz} = \sum_{j=1}^{N} Z_{ij}\sigma_j + V_{\infty z}$$

These equations are evaluated for every null point. The magnitude of the velocity V_i at each null point is then computed from

$$V_i = \sqrt{V_{ix}^2 + V_{iy}^2 + V_{iz}^2} \qquad (55)$$

and finally the pressure at each null point is computed. The loading pressure at any null point is based on an application of Bernoullis equation in the form

$$P_i = \frac{1}{2}\rho_b(V_{\infty_R}^2 - V_i^2) \qquad (56)$$

where V_R in this equation is defined as the magnitude of the onset flow evaluated at the coordinates of the center of impact.

With the simple onset flow model, negative pressures will be obtained for flat or nearly flat surfaces at

null points lying just outside of the projected area of the slice on the blade.[3] This occurs because the tangential velocity induced by an element in its own plane approaches infinity at the edges of the element. When the surface is flat, or nearly flat, the value of the source density for all null points lying outside of the immediate impact area is zero so that the net tangential velocity computed for these null points is heavily biased toward the tangential velocity induced at these null points by their nearest neighbor elements which lie under the projected area of the slice on the blade. In the current version of the loading model, if a negative pressure is computed, the negative value is ignored and a zero pressure is assumed instead.

3.2.9 Summary Description of Coupling Between Loading Model and Structural Dynamic Analysis

In loading used for any arbitrarily shaped impact surface, the impact area is divided into small flat elements, and a uniform distribution of sources is assumed to cover each area. At the beginning of impact, an initial pressure distribution is computed for the undeformed blade. During an impact in which local deformation takes place, the deformed shape of the impact zone is calculated in the dynamic structural analysis. After significant deformation has occurred, the geometry of the impact zone is provided to the loading model. The loading model is then used to calculate a new pressure distribution. As the structural analysis calculation proceeds, the local shape, the location, and the velocity of the impact area are updated and passed to the loading model at appropriate time intervals. The loading model, in turn, provides updated pressure distribution information for the structural response computation. The loading model is fully interactive with the structural response calculation. The duration of the impact is computed by keeping track of how much of the slice has been consumed during each time interval.

The loading model is capable of detailed interaction with the structural response model and of dealing with

target translation, rotation, and local deformation. The load-response coupling modelled in this formulation is capable of accurately predicting both overall target response and local deformation.

The principal limitation of the loading model, in its present form, is that it does not include transient effects of shock wave formation and decay. In birds, porosity appreciably reduces the peak pressures without significantly affecting steady flow pressures.[3,5] In addition, impact obliquity reduces the relative importance of shock pressures. Therefore, it is not obvious that neglect of the shock aspects of bird impact on blades is a significant deficiency. Nevertheless, efforts are currently being made to develop a simple, first order model for predicting the build up of the peak pressure to the Hugoniot pressure[3,5], and the decay of pressure from the peak pressure to the steady flow pressure by the combined action of release waves in the soft body and motion induced in the target material by the shock wave transmitted through the target material.

Preliminary work along these lines shows that the main effect of shocks during impacts on thin blades is to impact an initial deformation velocity to the blade material exposed to the slice. Thus, one approach to handling shock effects may be to simply model the initial impact process by imposing an initial velocity boundary condition to the blade material in the structural analysis. The appropriate initial velocity to be imported can be computed from a combination of Hugoniot pressure variables, dimensions of the slice, thickness of the blade material, and compressibility properties of the blade material.

SECTION 4
FOD LOADING MODEL COMPUTER PROGRAM

In this section the procedures used to translate the theoretical aspects of the surface singularity technique into a working computer program are presented. The input data and program options are described. Some details are given on how the basic loading model is interfaced with finite element structural analysis programs. Some results obtained with the loading model in the form of pressure distributions are presented along with comparisons to experimental results.

Some further theoretical developments associated with improved onset flow models are also presented. In particular, working equations for an onset flow model based on two-dimensional oblique jet impacts are developed and presented.

The loading model is set up so that non-slicing impacts can be considered as well as slicing impacts. No detailed experimental data, particularly pressure distributions, are available for slicing impacts. Thus, a non-slicing impact capability was created for the loading model to validate the output of the loading model computer program. Also, non-slicing capability was desired for investigating FOD impacts on non-rotating turbine engine components as well as aircraft external surfaces.

4.1 REFERENCE COORDINATE SYSTEM

While in principle any Cartesian coordinate system can be used with the surface singularity technique as developed in Section III, it was nevertheless found to be advantageous to work with a specific coordinate system for handling slicing impacts.

The coordinate system used in this report is one commonly used in the aircraft engine industry and is defined as follows: the Z axis is taken in the plane of rotation of the rotor with

z = 0 taken at the axis of rotation with positive z pointing from root to tip, the Y direction is parallel to (but not coincident with) the axis of rotation of the rotor and is positive when directed from the rear of the engine toward the front or inlet. The X axis is in the plane of rotation of the rotor and is perpendicular to the Z-axis. The positive x direction is defined so as to give a right-handed coordinate system. For a rotor viewed from the rear of the engine looking forward, positive rotational speed is defined as clockwise rotation. Thus, for positive rotational speed, the positive x-axis points in the direction of rotation. In short then, z is the radial direction, y is the forward direction, and x is the tangential direction. The origin of the coordinate system, except for z = 0, is not fixed to a specific location. With the coordinate system so defined, the program user can, in most cases, input a blade shape directly from design drawings generated in the aircraft engine industry.

4.2 DESCRIPTION OF INPUT DATA REQUIREMENTS

The primary input variables have already been defined in Sections II and III. They are restated in this section along with the symbols used in the loading model to define these quantities.

4.2.1 Input Data for Slicing Impacts

There are three options for slicing impacts. The input variable ISLICE is used to define the type of object being sliced. ISLICE = 1 denotes a bird, ISLICE = 2 denotes an ice sphere, and ISLICE = 3 denotes an ice slab. The definitions of the input variables for a slicing impact of a bird are given in Table III. Most of the impact variables defined in Table III are used in all three options. For an ice sphere only the definitions of V_b and W_b are changed. For an ice sphere, V_b is taken as the axial speed of the sphere (aircraft speed) and W_b is the mass of the ice sphere. For an ice slab the user must input for V_b the axial velocity of the slab relative

TABLE III

DEFINITION OF INPUT DATA FOR SLICING BIRD IMPACT.

Variables	Symbol Used in Report	Symbol Used in Computer Program
No. of blades per stage	N	NBL
Blade rotational speed (rpm)	n	RPMY
Axial speed of the bird (user generally specifies this as the aircraft speed)	V_b	VB
Bird weight	W_b	WB
Radius on rotor at which impact occurs	Z_i	RI
Time at which impact begins	-	TIM
Coordinates of blade leading edge at Z_i	-	(XL, YL)
Coordinates of blade trailing edge at Z_i	-	(XT, YT)
No. of chordwise cuts on the blade for the purpose of generating a grid system	NC	NC
No. of spanwise cuts on the blade for the purpose of generating a grid system	NS	NS
Mass density of the bird	ρ_L	RHOB

to the engine nacelle (a number generally less than the aircraft speed but greater than zero). Also for an ice slab the user must supply as input the length of the ice slab (BL) and the height of the slab (DB); where height denotes how much of the span of the blade is to be exposed to the slab. The thickness of the slice taken out of the slab is not an input number but is taken to be the maximum possible slice width, h, computed in equation 7.

The coordinates of the leading and trailing edge points defined in Table III are used to define the blade orientation angle δ defined in Figure 2.

$$\delta = \tan^{-1} [(YL-YT)/(XL-XT)] \qquad 57$$

4.2.2 Input Data for Non-Slicing Impacts

For non-slicing impacts, a right circular cylinder with L = 2D is assumed. A value of one for NEL should be inputed to signal that non-slicing impact is occurring. The location of the center of impact (XI, YI, ZI) is then read in as input data along with the three velocity components of the projectile.

4.3 MAJOR PROGRAM VARIABLE NAMES

A list of the major program variable names is given in Appendix A.

4.4 INTERFACING DETAILS

In the present version of the loading model program the following decisions are assumed to be made in the structural analysis program:

(1) the time at which a pressure distribution is to be computed by the loading model

(2) the number of chordwise cuts NC and spanwise cuts NS to be made on the blade for the purpose of generating a grid system on the impact area

(3) the surface nodal locations where pressures are to be computed

Whenever the structural analysis computer program decides that an updated pressure distribution is required, the above information is supplied to the loading model computer program (called BPRESS). The displacement velocities at the surface nodal locations where pressures are to be computed are also supplied to BPRESS. With this information BPRESS computes the following: first, the corner points of the plane quadrilateral elements are computed according to the scheme outlined in Section 3.2.1. Then the element on which the center of impact occurs is determined. This is done by searching for the one

surface element which is intersected by the line defining the path of the axis of symmetry of the impacting object. Next the velocity of the impacting object relative to the element on which the center of impact occurs is computed taking into account the displacement velocity of this element. This relative velocity is used to define the instantaneous dynamic pressure of the impact and is also used to compute the amount of impacting object consumed during the time interval between the previous call to BPRESS and the current call to BPRESS (DLC). The amount of object which is not yet consumed (BLR) and the (current best estimate of the time at which the entire object will have been consumed (TERM) are computed.

The vector matrix of influence coefficients are next computed (Section 3.2.5) followed by computation of the onset flow. The onset flow computation includes the effect of displacement velocities. The system of linear equations which determine the set of source densities (Section 3.2.7) is then solved. The final major computation in BPRESS is the computation of flow velocities and pressure at the surface nodal points which are approximately equivalent to the null points. The pressures and the estimated time of impact durations are then returned to the structural analysis executive routine.

4.5 PRESSURE DISTRIBUTIONS OBTAINED WITH THE LOADING MODEL

4.5.1 Oblique Impacts on Rigid Surfaces

At the present time, steady-state experimental pressure distributions are available only for real and substitute birds impacting on rigid flat plates. Figure 9 shows a comparison between computed and measured steady-state pressure distributions for a 45 degree impact angle. The distribution shown in Figure 9 is along the major axis. Figure 10 shows the same type of comparison but for a more oblique impact (25 degrees). Figure 11 shows pressure distributions along the minor axis for 45 and 25 degree impacts. The

computed results shown in these three Figures are based on the simple onset flow model which was described in Section 3.1.2. The limitations of this simple onset flow model are clearly evident from these figures where it is observed that in the low pressure region, near the edges of the projected area of the bird on the plate, the computed pressure distribution is not in agreement with the measured distribution. However, it can be seen that the agreement between theoretical and experimental results is excellent over the impact region where the pressures are large. Many attempts have been made in the course of this effort to develop better onset flow models which lead to improved pressure distributions at the edge of the projected area of the projectile on the impact surface. Except for normal or nearly normal impacts, no reasonably simple onset flow model has been discovered which yields better overall results than the very simplest model, that is, the one used to generate the results shown in Figures 9, 10, and 11.

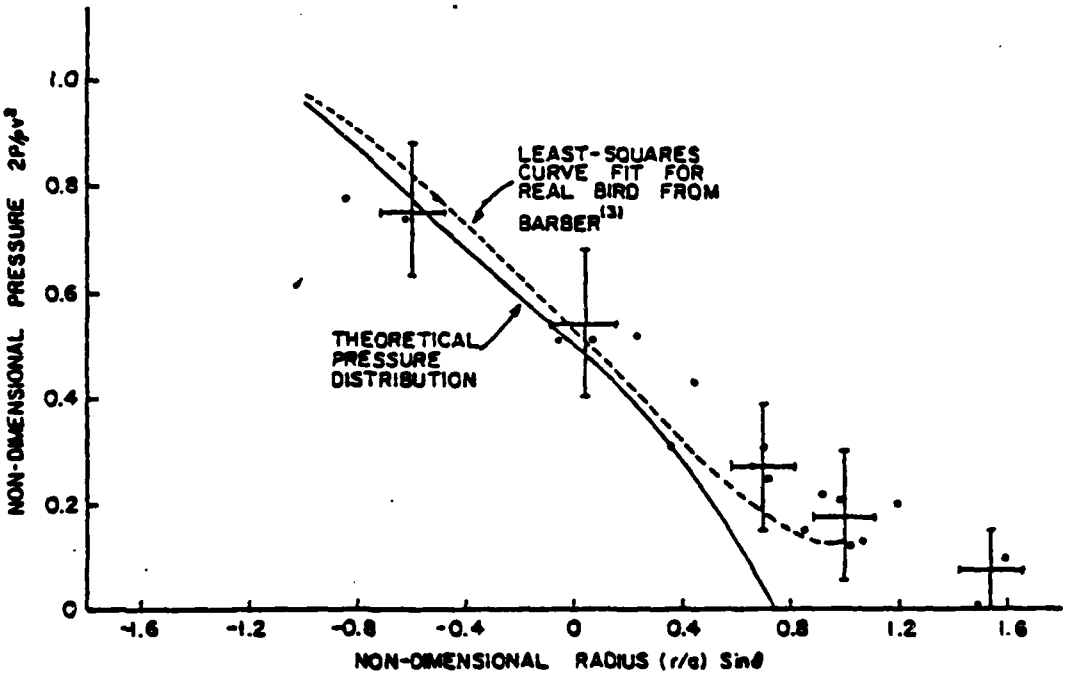

Figure 9. Normalized Steady Flow Pressure Distribution of Nominal 1800 g Real Bird (chicken) Along Major Axis at 45 Degree Impact

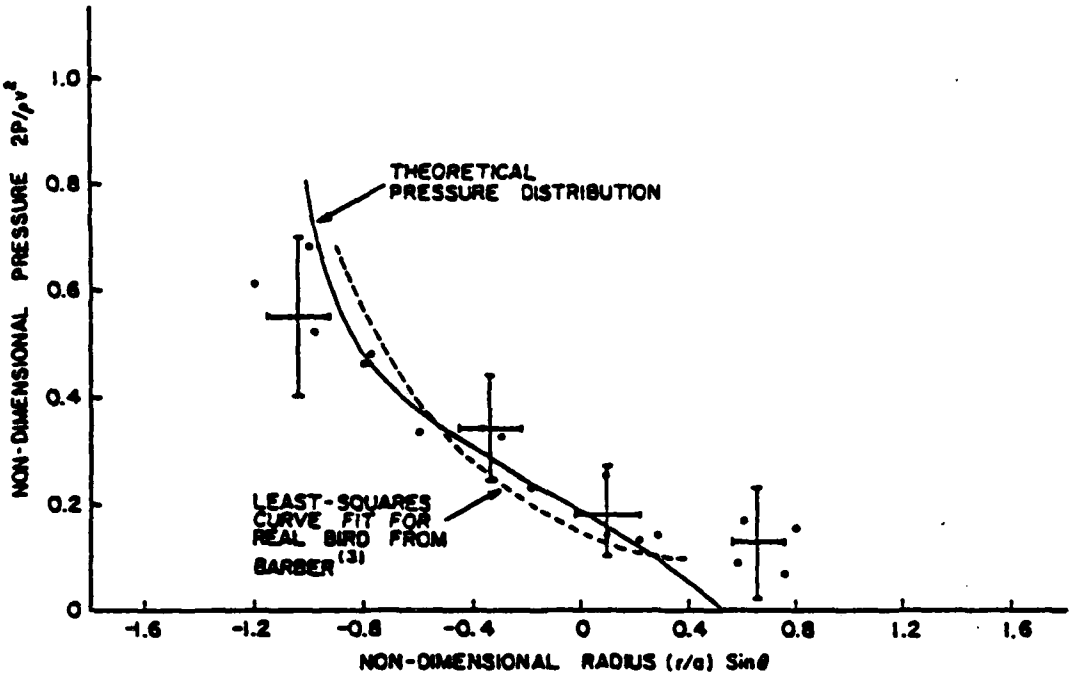

Figure 10. Normalized Steady Flow Pressure Distribution of Nominal 1800 g Real Bird (chicken) Along Major Axis at 25 Degree Impact

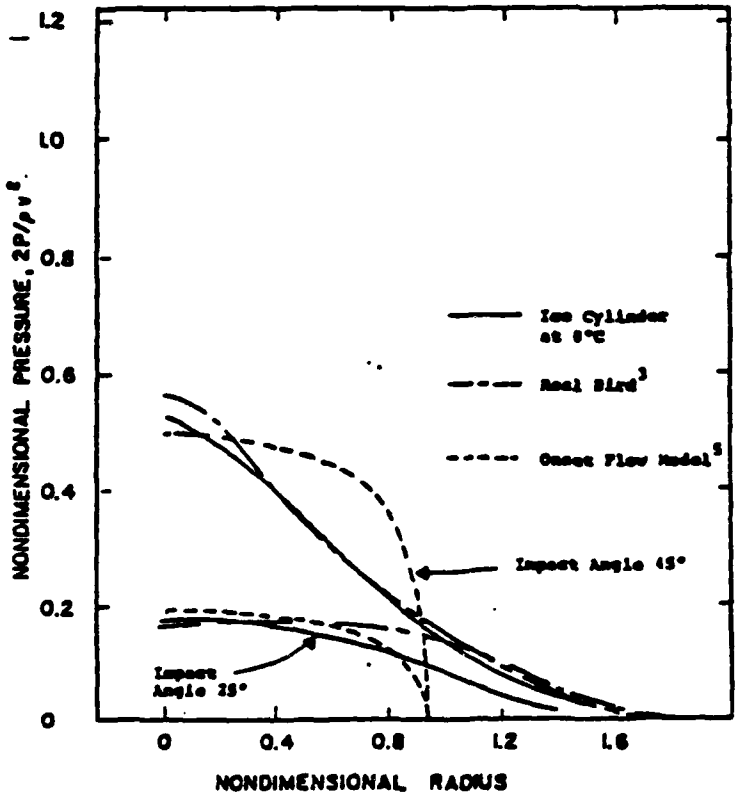

Figure 11. Comparison of Steady Flow Pressure Distributions Along Minor Axis for Ice; Real Birds; and Loading Model

4.5.2. Normal Impacts on Rigid Surfaces

Figure 12 shows the pressure distribution obtained with the loading model using the simple onset flow description. Experimental data points are also shown in Figure 12 along with the theoretical pressure distribution for a two-dimensional jet. The results shown in Figure 12 clearly show that the simple onset flow description is not adequate for normal impacts. The total force impacted to the impact surface corresponding to the simple onset flow is only about one-half of the theoretical value of $\rho V_b A$ where A is the cross-sectional area of the projectile. The pressure distribution for a two-dimensional jet led to a gross over-estimate of the total impact force. An approximate theoretical pressure distribution for an axisymmetric normal jet impact developed by Schach [7] is also shown in Figure 12 along with Schach's measured pressure distribution.

In the next section an improved onset flow model based on a two-dimensional jet theoretical solution is presented which yields excellent agreement with experimental pressure distributions.

4.6 AN IMPROVED ONSET FLOW MODEL FOR NORMAL IMPACTS

The inadequacy of the simple onset flow description for normal impacts is due to the fact that the spreading of the edge of the fluid jet as it approaches the impact surface is not taken into account. For oblique impacts this is not a serious shortcoming since the major portion of the jet is deflected from its oncoming path on that portion of the impacted area which lies within the projected area of the projectile on the impact surface. For normal impacts, however, much of the momentum transfer occurs outside of the projected area of the projectile on the impact surface.

Figure 13 shows a comparison of the jet boundary free streamline shapes for normal impact of two-dimensional and axisymmetric jets. This figure shows that the turning of an

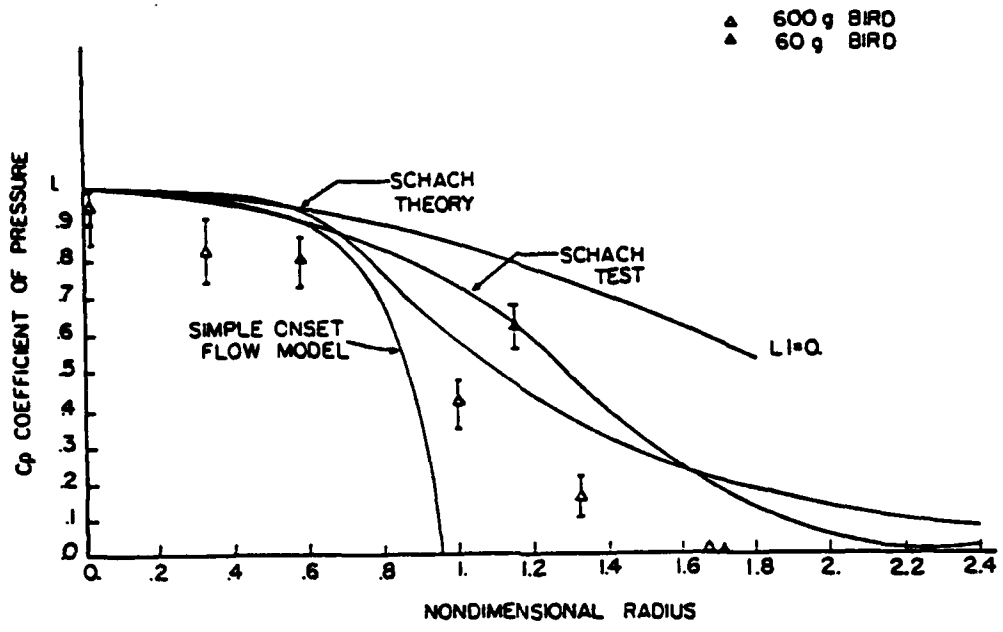

Figure 12. Comparison of Steady Flow Pressure Distributions Along Major Axis for Normal Impacts

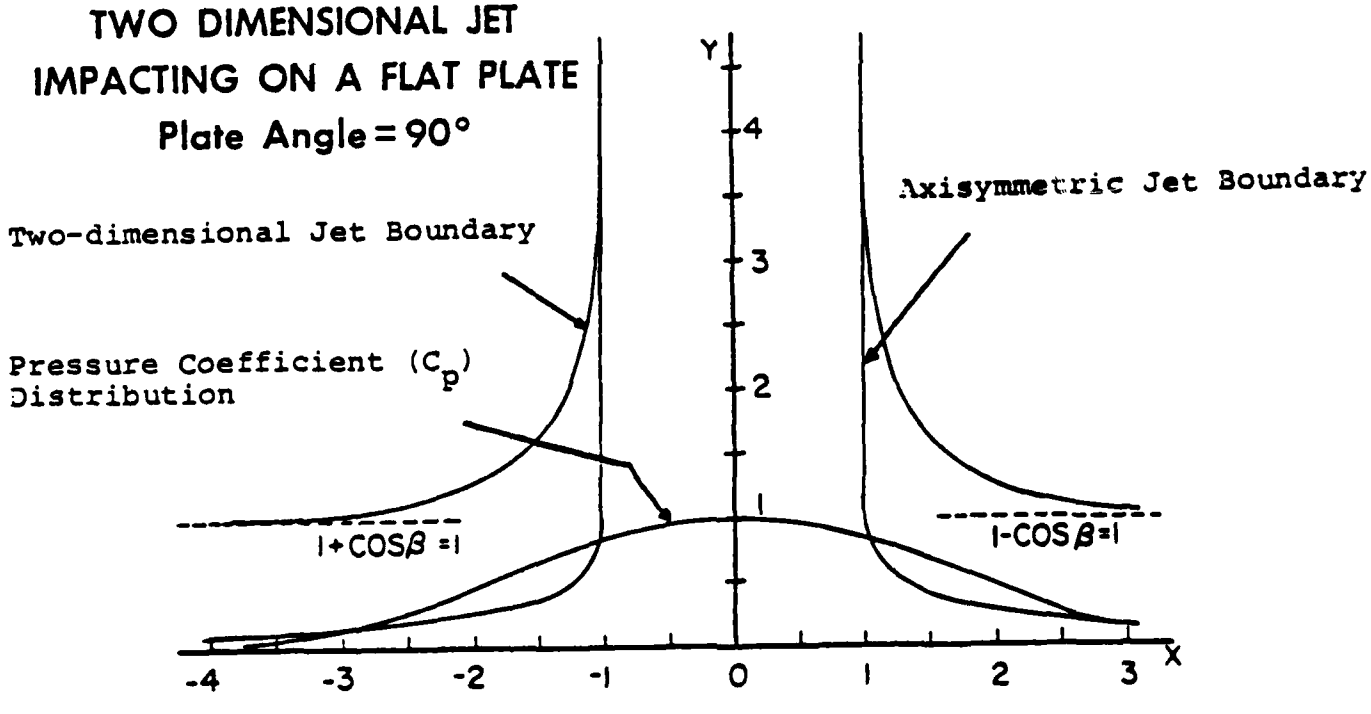

Figure 13. Comparison of Jet Boundaries for Two-Dimensional and Axisymmetric Jets

axisymmetric jet is much more abrupt than the turning of a two-dimensional jet. From Figure 13 it is observed that the two-dimensional jet boundary streamlines are not altogether dissimilar from the axisymmetric jet if the Y axis of the two-dimensional jet is shifted downward by an amount equal to the jet half-width. This observation led to the following question. Suppose the two-dimensional jet velocity field evaluated at Y/a in the vicinity of 1 was used as an onset flow description. Is it possible to find some value of Y/a that has a velocity field which when used as an onset flow description would yield a pressure distribution similar to the axisymmetric pressure distribution? Figure 14 shows pressure distribution that correspond to various values of Y/a (denoted by L1 on Figure 14). From comparison of Figure 14 to Figure 12, it can be seen that the pressure distribution for Y/a (L1) 1.25 is remarkably close to the measured axisymmetric pressure distribution. Thus if the two-dimensional jet velocity field evaluated at a non-dimensional distance from the impact surface of Y/a = 1.25 is used as an onset flow description, a reasonably accurate pressure distribution for axisymmetric normal impacts on rigid flat plates can be obtained. In the present version of the loading model computer program, this improved onset flow description is used instead of the simple onset flow description when normal impacts are considered. The theoretical solution for the velocity field of the two-dimensional jet impacting on a rigid flat plate at an incidence angle β is presented in Appendix B, equations B-8 and B-9. For a normal impact (β = 90 degrees), it was found that, at Y/a = 1.25, the normal component of velocity is approximately constant over the jet width and is equal to

$$V' = 0.5 \qquad 58$$

and the tangential velocity distribution given by

$$U' = 0.9\ (1 - e^{-(x/a)}) \qquad 59$$

Equations 58 and 59 are used to describe the onset flow velocity field for normal impacts rather than the exact two-dimensional

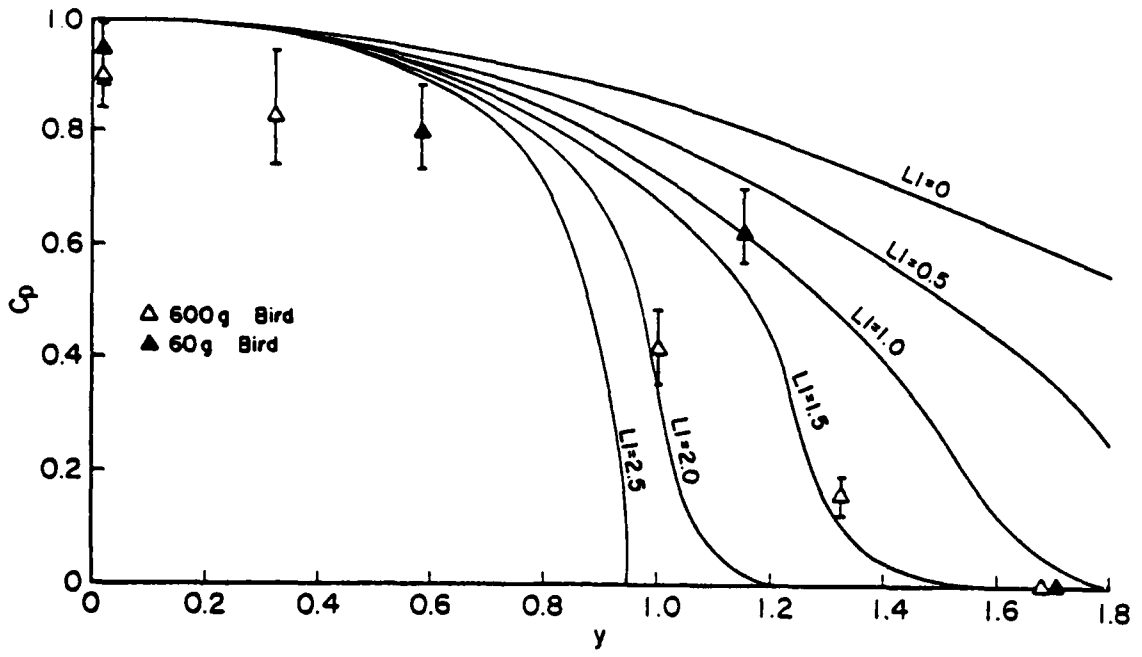

Figure 14. Comparison of Pressure Distributions for Normal Impacts

velocity solution, which must be solved iteratively.

When using the loading model for normal impacts, the user must define the impact area to be at least 1.8 times the projectile radius in order to obtain a pressure distribution, which gives a total impulse within 90 percent of the theoretical value.

One may question the need of using the loading model computer program for normal impacts of cylindrical projectiles. Why not simply use the pressure distribution for axisymmetric jets given in Figure 13. For normal impacts on rigid flat surfaces an emperical equation for the pressure distribution would certainly be a much simpler approach. However, for normal impacts on deformable surfaces one cannot use a rigid flat plate pressure distribution to describe the loading. The present improved onset flow model using equation 59 to represent the velocity tangent to the deformed surface has been found to correctly describe the loading effects produced by pocketing or cupping of the impact area on deforming surfaces.

4.7 ONSET FLOW MODELING FOR OBLIQUE IMPACTS

A large amount of effort has been expended in attempts to generate improved onset flow models for oblique models. Much of this effort has centered on using two-dimensional jet theoretical velocity field solutions in one form or another to model the onset flow. While it has been possible to use two-dimensional jet theory to develop onset flow description, which yield pressure distribution that agree with the measured pressure distributions for oblique impacts on rigid flat plates than is possible with the simple onset flow model, these efforts have not produced acceptable results for the following reason. The programming and computer time required to compute the improved onset flow velocity field becomes very large, to the point where the onset flow computation becomes the major computation.

The simple onset flow model yields acceptable results for impact angles less than or equal to 45 degrees. For normal or nearly normal impacts (90 and 75 degrees) the improved onset flow model discussed in the previous section has been found to yield acceptable results. Thus at the present time no relatively simple onset flow model is available for impacts over the 45 to 60 degree incidence angle range. At the present time this is not a serious limitation to the scope of the work of the contractual effort since angles of incidence in the 45 to 75 degree are not encountered in high performance turbine engines (see Tables I and II for APSI and F-101 engine Bird-Blade Incidence angles).

4.8 ADDITIONAL PROGRAMMING FOR NON-SLICING IMPACTS

As was mentioned in Section 4.2.2, when the loading model is used for non-slicing impacts, the location of the center of impact and velocity components of the projectile are specified by the user. The methods used to treat this type of impact are identical to those developed by the authors of this report for treating impacts on aircraft transparencies and are discussed in Appendix C.

APPENDIX A
SYMBOL DEFINITION

APPENDIX A
SYMBOL DEFINITION

In this appendix the symbols used in the program will be defined and related to the equations derived or listed in Section 3.

N	:	number of elements
XN(I),YN(I),ZN(I)	:	X, Y, and Z coordinates of the input points defining the shape of the impact surface.
UX(I),UY(I),UZ(I)	:	X, Y, and Z components of the velocity at the null point
X(1,I),X(2,I),X(3,I),X(4,I)	:	X coordinates of the corner points forming the element
Y(1,I),Y(2,I),Y(3,I),Y(4,I)	:	Y coordinates of the corner points forming the element
Z(1,I),Z(2,I),Z(3,I),Z(4,I)	:	Z coordinates of the corner points forming the element
T1X,T1Y,T1Z	:	components of the diagonal vector $\vec{T}_1$ joining corners 1 and 3
T2X,T2Y,T2Z	:	components of the diagonal vector $\vec{T}_2$ joining corners 2 and 4
XN1,YN1,ZN1	:	components of the cross product vector $\vec{N}$ of the two diagonal vectors

UNX,UNY,UNZ : components of the unit normal vector $\vec{n}$

XAV,YAV,ZAV : coordinates of the average point of the four corner points of the element

D1,D2,D3,D4 : signed projection distance of the four input points used to form an element into the plane of the element

XP1,XP2,XP3,XP4 : X coordinates of the corner points of the quadrilateral element in the reference coordinate system

YP1,YP2,YP3,YP4 : Y coordinates of the corner points of the quadrilateral element in the reference coordinate system

ZP1,ZP2,ZP3,ZP4 : Z coordinates of the corner points of the quadrilateral element in the reference coordinate system

T1 : magnitude of the diagonal vector $\vec{T}_1$

TP1X,TP1Y,TP1Z : components of the unit vector $\vec{t}_1$ in the reference coordinate system used to define the element coordinate system

TP2X,TP2Y,TP2Z : components of the unit vector $\vec{t}_2$ in the reference coordinate system used to define the element coordinate system

ZETAP1,ZETAP2,ZETAP3,ZETAP4	:	ZETA coordinates of the corner points of the quadrilateral element in the element coordinate system using the average point as origin
ETAP1,ETAP2,ETAP3,ETAP4	:	ETA coordinates of the corner points of the quadrilateral element in the element coordinate system using the average point as origin
ZETAOR,ETAOR	:	coordinates of the centroid in the element coordinate system using the average point as origin
ZETA1,ZETA2,ZETA3,ZETA4	:	ZETA coordinates of the corner points of the quadrilateral element in the element coordinate system using the centroid as origin
ETA1,ETA2,ETA3,ETA4	:	ETA coordinates of the corner points of the quadrilateral element in the element coordinate system using the centroid as origin
XO,YO,ZO	:	coordinates of the centroid of the quadrilateral element in the reference coordinate system
XX,YY,ZZ	:	coordinates of the calculated null point in the element coordinate system

D12,D23,D34,D41 : length of the four sides of the quadrilateral element which are given in Equation 43

R1,R2,R3,R4 : quantities defined by Equation 45

U11,U22,U33,U44 : the X components of the velocity induced by a side of the quadrilateral element at a null point

XU1,YV1,ZW1 : X, Y, and Z components of the velocity induced by a quadrilateral element at a null point

V11,V22,V33,V44 : the Y components of the velocity induced by a side of the quadrilateral element at a null point

W11,W22,W33,W44 : Z components of the velocity induced by a side of the quadrilateral element at a null point

R1R2X,R2R3X,R3R4X,R4R1X
R1R2Y,R2R3Y,R3R4Y,R4R1Y
DD12,DD23,DD34,DD41 : quantities used to evaluate the partial derivatives of V_x and V_y (Equation 48) with respect to x and y

VXX,VXY : partial derivatives of the X component of the induced velocity V_x with respect to X and Y

VYX,VYY : partial derivatives of the Y component of the induced velocity V_y with respect to X and Y

DELX,DELY	:	change in value of the coordinates of the null point produced by one iteration in the solution of the non-linear equations for the null point
XPNP,YPNP,ZPNP	:	coordinates of the null point of the quadrilateral element in the reference coordinate system
XNP,YNP,ZNP	:	coordinates of the i-th null point in the j-th element coordinate system
ZE21,ZE32,ZE43,ZE14	:	X components of the length of the sides of the quadrilateral element
ET21,ET32,ET43,ET14	:	Y components of the length of the sides of the quadrilateral element
E1,E2,E3,E4 H1,H2,H3,H4 M12,M23,M34,M41	:	quantities defined by Equations 44, 46, and 47
UPX,VPY,WPZ	:	velocity components induced at the null point of the i-th element by a unit source density on the j-th element in the reference coordinate system
AN(I,J)	:	induced normal velocity at the null point of the i-th element by a unit source density on the j-th element (Equation 49)

VINFX,VINFY,VINFZ	:	components of a uniform onset flow in the reference coordinate system
ON(I)	:	normal component of a uniform onset flow at the null point of the i-th element (Equation 52)
S(I)	:	source density on the i-th quadrilateral element
T1,T2,T3	:	components of the velocity induced at the null point of the i-th element by a source density S(J) on the j-th element in the reference coordinate system
U1,V1,W1	:	components of the total flow velocity at the null point of the i-th element in the reference coordinate system
VEL	:	magnitude of the total flow velocity at the null point of the i-th element
CP	:	pressure coefficient at a null point
P(I)	:	pressure magnitude at the null point of the i-th element

APPENDIX B
TWO-DIMENSIONAL ONSET FLOW MODELING

APPENDIX B
TWO-DIMENSIONAL ONSET FLOW MODELING

To find the exact source density on the quadrilateral elements, the onset flow needs to be specified. A two-dimensional onset flow was modeled and found adequate to use with axisymmetric jet impacting on flat surfaces at oblique angles. The onset flow is assumed to be a two-dimensional jet flow bounded by free streamlines, impacting on a flat surface. A free streamline is a streamline which separates fluid in motion from fluid at rest and is a line of constant speed and pressure. To completely specify the onset flow, the boundary of the jet, which is composed of free streamlines, along with the velocity field and the stagnation point need to be derived.

B-1 DERIVATION OF VELOCITY FIELD EQUATIONS

The velocity on the free streamline is complex and denoted by υ and written as:

$$\upsilon = U - iV \tag{B-1}$$

Milne-Thomson expressed Z, where $Z = x + iy$, in terms of υ, of two impinging jets A_1 and A_2, meeting and branching off into two other streams B_1 and B_2 (see Figure B-1) as:

$$Z = \frac{U}{\pi}\left\{\frac{h_1}{a_1}\log\left(1-\frac{\upsilon}{a_1}\right)+\frac{h_2}{a_2}\log\left(1-\frac{\upsilon}{a_2}\right)\right.$$
$$\left.-\frac{K_1}{b_1}\log\left(1-\frac{\upsilon}{b_1}\right)-\frac{K_2}{b_2}\log\left(1-\frac{\upsilon}{b_2}\right)\right\} \tag{B-2}$$

where h_1, h_2, K_1, and K_2 denote the breadths at infinity of A_1, A_2, B_1, and B_2; and $a_1 = U$, $a_2 = Ue^{i\alpha}$, $b_1 = Ue^{i\beta}$, and $b_2 = Ue^{i\gamma}$. β is the angle between A_1 and B_1, α is the angle between A_1 and A_2, and γ is the angle between A_1 and B_2. The expression for Z shows that the motion is reversible. For our purposes, consider the direct impact of two jets with the same asymptote as shown in

Figure B-2. Assume that A_1 and A_2 are two uniform streams, then the inflow and outflow must balance to preserve continuity.

$$h_1 + h_2 = K_1 + K_2 \tag{B-3}$$

From conservation of momentum in the x and y directions we obtain:

$$h_1 + h_2 \cos\alpha - K_1 \cos\beta - K_2 \cos\gamma = 0$$

$$h_2 \sin\alpha - K_1 \sin\beta - K_2 \sin\gamma = 0 \tag{B-4}$$

Now it is clear that a symmetrical solution must exist. Thus

$$K_1 = K_2 , \quad \alpha = \pi , \quad \gamma = 2\pi - \beta$$

From Equations B-4 and B-3

$$\text{Cos}\,\beta = \frac{h_1 - h_2}{K_1 + K_2}$$

and $$h_1 + h_2 = 2K_1.$$

Solving for h_1 and h_2 we found that

$$h_1 = K_1 (1 + \cos\beta)$$

$$h_2 = K_1 (1 - \cos\beta) \tag{B-5}$$

Substituting these values in the expression of Z in Equation B-2 we get:

$$Z = \frac{K_1}{\pi}\left\{(1+\cos\beta)\log\left(1-\frac{u-iv}{U}\right)-(1-\cos\beta)\log\left(1+\frac{u-iv}{U}\right)\right. \tag{B-6}$$

$$\left. -\frac{1}{e^{i\beta}}\log\left(1-\frac{u-iv}{Ue^{i\beta}}\right)-\frac{1}{e^{i(2\pi-\beta)}}\log\left(1-\frac{u-iv}{Ue^{i(2\pi-\beta)}}\right)\right\}$$

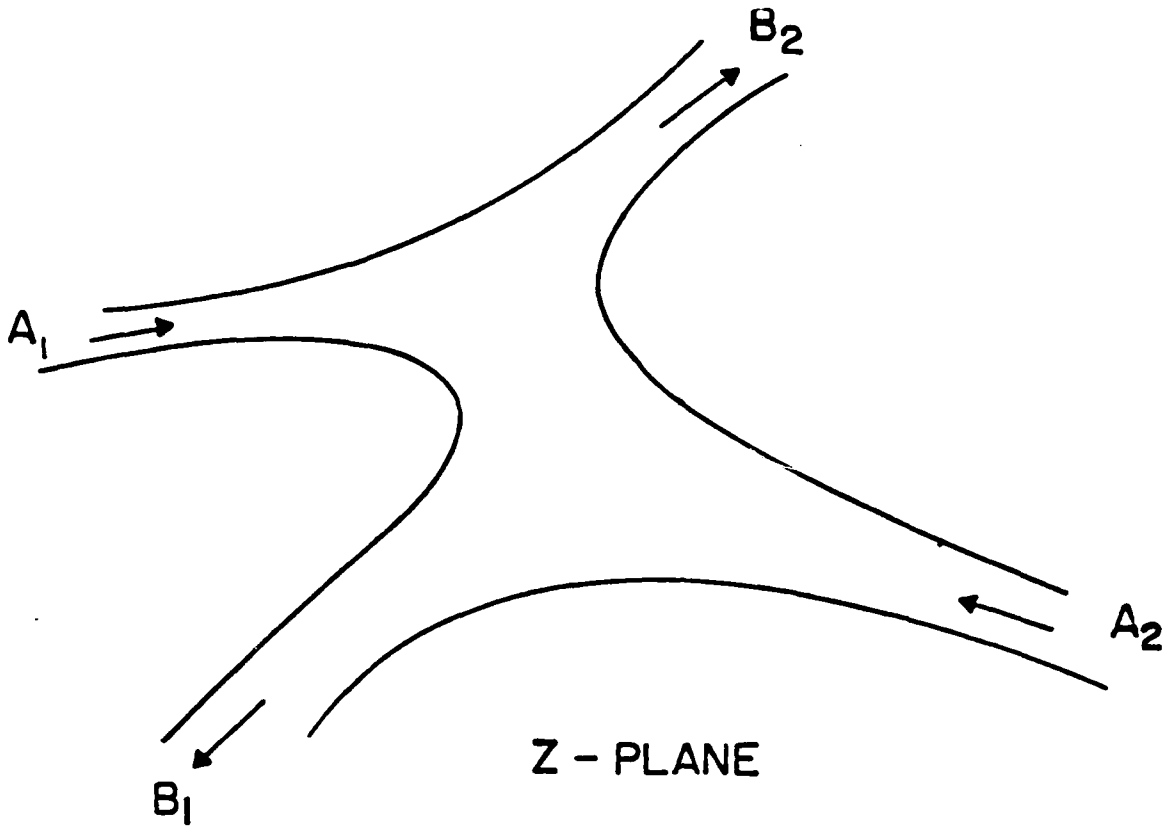

Figure B-1. Z-Plane

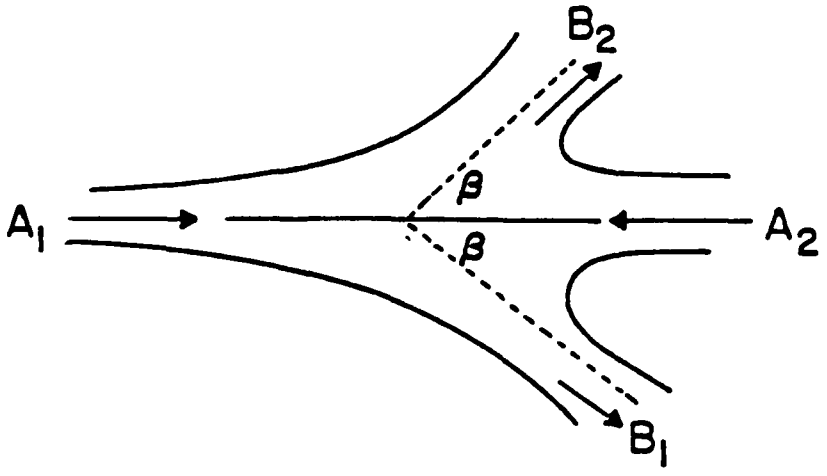

Figure B-2. Two Jets with the Same Asymptote Impinging Directly

From reversibility and symmetry, it is obvious that solving Equation B-6 for u and v will give us the onset flow needed.

Non-dimensionalizing the velocities u and v by the magnitude of the impacting flow U, we get:

$$Z = \frac{K_1}{\pi}\left\{ \log\left[\frac{1-u'+iv'}{1+u'-iv'}\right] + \cos\beta \log\left[(1-u'+iv')(1+u'-iv')\right] \right.$$
$$-(\cos\beta - i\sin\beta)\ \log\left[1-(u'-iv')(\cos\beta - i\sin\beta)\right]$$
$$\left. -(\cos\beta + i\sin\beta)\ \log\left[1-(u'-iv')(\cos\beta + i\sin\beta)\right]\right\} \qquad \text{(B-7)}$$

where $u' = u/U$ and $v' = v/U$. Rearranging Equation B-7 and equating it with $Z = x + iy$ gives:

$$\frac{X}{k_1/2} = \frac{2}{\pi}\left\{ \log\left[\frac{\sqrt{(1-u')^2+v'^2}}{\sqrt{(1+u)^2+v'^2}}\right] \right. \qquad \text{(B-8)}$$
$$+\cos\beta \log\left[\frac{\sqrt{(1-u')^2+v^2}\sqrt{(1+u')^2+v'^2}}{\sqrt{(1+v'\sin\beta-u'\cos\beta)^2+(u'\sin\beta+v'\cos\beta)^2}}\right]$$
$$-\cos\beta \log\sqrt{(1-v'\sin\beta-u'\cos\beta)^2+(v'\cos\beta-u'\sin\beta)^2}$$
$$-\sin\beta\left[\tan^{-1}\left[\frac{(u'\sin\beta+v'\cos\beta)}{(1-u'\cos\beta+v'\sin\beta)}\right]\right.$$
$$\left.\left. -\tan^{-1}\left[\frac{(v'\cos\beta-u'\sin\beta)}{(1-u'\cos\beta-v'\sin\beta)}\right]\right]\right\}$$

$$\frac{y}{k_1/2} = \frac{2}{\pi}\left\{ \tan^{-1}\left(\frac{v'}{1-u'}\right) - \tan^{-1}\left(\frac{-v'}{1+u'}\right) + \cos\beta\left[\tan^{-1}\left(\frac{v'}{1-u'}\right) \right.\right. \tag{B-9}$$

$$+ \tan^{-1}\left(\frac{-v'}{1+u'}\right)$$

$$\left. - \tan^{-1}\left(\frac{u'\sin\beta + v'\cos\beta}{1-u'\cos\beta+v'\sin\beta}\right) - \tan^{-1}\left(\frac{v'\cos\beta - u'\sin\beta}{1-u'\cos\beta - v'\sin\beta}\right)\right]$$

$$\left. + \frac{\sin\beta}{2}\left[\log\frac{(1+v'\sin\beta - u'\cos\beta)^2 + (u'\sin\beta + v'\cos\beta)^2}{(1-v'\sin\beta - u'\cos\beta)^2 + (v'\cos\beta - u'\sin\beta)^2}\right]\right\}$$

Now the velocities u' and v' can be calculated, for any point within the boundary with coordinates x and y, by solving simultaneously the two non-linear Equations (B-8) and (B-9). These equations are solved by means of an iterative procedure.

The iterative procedure is as follows. Let U'_p and V'_p denote the p-th approximation of the velocity components u' and v' of any point with known coordinates x and y. The (p+1)-th approximation is obtained by solving for U'_{p+1} and V'_{p+1} in the pair of linear algebraic equations

$$-\delta_1(u',v') = \left[\frac{\partial\delta_1}{\partial u'}\right]^{(P)}\left(U'_{p+1} - U'_p\right) + \left[\frac{\partial\delta_1}{\partial v'}\right]^{(P)}\left(V'_{p+1} - V'_p\right) \tag{B-10}$$

$$-\delta_2(u',v') = \left[\frac{\partial\delta_2}{\partial u'}\right]^{(P)}\left(U'_{p+1} - U'_p\right) + \left[\frac{\partial\delta_2}{\partial v'}\right]^{(P)}\left(V'_{p+1} - V'_p\right)$$

The iterative procedure is terminated when the functions δ_1 and δ_2 are both less in absolute value than a small prescribed value. The iterative procedure replaces the non-linear Equations (B-8) and (B-9) by linear Equations (B-10), whose coefficients are the derivatives of the non-linear functions. In Equation (B-10) δ_1 and δ_2 are non-linear functions of U' and V'.

$$\delta_1(u',v') = \frac{x}{k_1/2} - \frac{2}{\pi}\left\{\frac{1}{2}\log\left[\frac{(1-u')^2+v'^2}{(1+u')^2+v'^2}\right]\right.$$

$$+\frac{1}{2}\cos\beta\left[\log\frac{\left[(1-u')^2+v'^2\right]\left[(1+u')^2+v'^2\right]}{(1+u'^2+v'^2+2v'\sin\beta-2u'\cos\beta}\right.$$

$$\left.\left.-\log(1+u'^2+v'^2-2v'\sin\beta-2u'\cos\beta)\right]\right.$$

$$\left.-\sin\beta\tan^{-1}\left[\frac{2u'\sin\beta-2(u'^2+v'^2)\cos\beta\sin\beta}{1-(u'^2+v'^2)(\sin^2\beta-\cos^2\beta)-2u'\cos\beta}\right]\right\} \qquad \text{(B-11)}$$

$$\delta_2(u',v') = \frac{y}{k_1/2} - \frac{2}{\pi}\left\{\frac{\sin\beta}{2}\log\left[\frac{1+u^2+v^2+2v\sin\beta-2u\cos\beta}{1+u^2+v^2-2v\sin\beta-2u\cos\beta}\right]\right.$$

$$+\cos\beta\left[\tan^{-1}\left[\frac{2u'v'}{1-(u'^2-v'^2)}\right]-\tan^{-1}\left[\frac{2v'\cos\beta-2u'v'}{1+u'^2-v'^2-2u'\cos\beta}\right]\right]$$

$$\left.+\tan^{-1}\left[\frac{2v'}{1-(u^2+v'^2)}\right]\right\} \qquad \text{(B-12)}$$

The convergence is fairly rapid but care should be taken while evaluating the arc tangents. They should be evaluated between $-\pi$ and π.

B-2 BOUNDARY OF THE JET

Consider the flow described in Figure B-2, let the x-axis be along the line of impact and the origin be the stagnation point of the two flows when they meet and branch into a 90 degree angle. If we regard the streamline $y = 0$ as a rigid barrier, we will get a two-dimensional jet flow impacting on an infinite plate at an oblique angle, which is the case we are studying (Figure B-3) and lets divide the flow in two regions, Region 1 from the centerline of the jet toward the positive x-axis and Region 2 toward the negative x-axis. On a free streamline, the complex velocity

$$\nu = U e^{-i\theta} \tag{B-13}$$

If we substitute this in the expression for Z in Equation (B-2); and equate the real and imaginary parts, we get the coordinates (x,y) of a point on the free streamlines expressed in terms of the parameter θ. Substituting in Z we get:

$$Z = \frac{1}{\pi}\left\{ \frac{i}{2}\left(- h_2 \alpha e^{-i\alpha} + K_1 \beta e^{-i\beta} + k_2 \gamma e^{-i\gamma}\right) + h_1 \log\left(\sin\frac{\theta}{2}\right)\right.$$

$$+ h_2 e^{-i\alpha} \log\left(\sin\frac{\theta+\alpha}{2}\right) - k_1 e^{-i\beta} \log\left(\sin\frac{\theta+\beta}{2}\right) \tag{B-14}$$

$$\left. - k_2 e^{-i\gamma} \log\left(\sin\frac{\theta+\gamma}{2}\right)\right\}$$

Substituting the values of h_1, h_2, K_1, K_2, α and γ, calculated from Equations B-3, B-4, and B-5 into Equation B-14 will give us the expression for Z of interest in our problem, which is:

$$Z = \frac{K_1}{\pi}\left\{\log\left(-i\tan\left(\frac{-\theta}{2}\right)\right) + \cos\beta\,\log\left(\frac{i\sin\theta}{2}\right)\right.$$

$$+\left(\cos\beta - i\sin\beta\right)\left[\left(\beta - \frac{\pi}{2}\right)i + \log\left(-i\,\frac{\sin\left[\left(\frac{\pi}{4}-\frac{\theta}{2}\right)-\left(\frac{\pi}{4}-\frac{\beta}{2}\right)\right]}{\cos\left[\left(\frac{\pi}{4}-\frac{\theta}{2}\right)+\left(\frac{\pi}{4}-\frac{\beta}{2}\right)\right]}\right)\right]$$

$$\left. - 2\cos\beta\left[\frac{i\beta}{2} + \log\left(-i\sin\left[\left(\frac{\pi}{4}-\frac{\theta}{2}\right)-\left(\frac{\pi}{4}-\frac{\beta}{2}\right)\right]\right)\right]\right\} \qquad \text{(B-15)}$$

In region 1 θ is between $-\pi$ and $-(2\pi-\beta)$, let $\chi = -\pi-\theta$, then $\theta = -\pi-\chi$ and $\chi/2$ will be between zero and $\pi/2$ minus $\beta/2$. By substituting θ by its value in Equation (B-15) we get:

$$Z = \frac{K_1}{\pi}\left\{\log\left(i\cot\frac{\chi}{2}\right) + \cos\beta\,\log\left(i\frac{\sin\chi}{2}\right) + \left(\cos\beta - i\sin\beta\right)\left[\left(\beta-\frac{\pi}{2}\right)i\right.\right.$$

$$\left. + \log\left[-i\,\frac{\sin\left[\left(\frac{3\pi}{4}+\frac{\chi}{2}\right)-\left(\frac{\pi}{4}-\frac{\beta}{2}\right)\right]}{\cos\left[\left(\frac{3\pi}{4}+\frac{\chi}{2}\right)+\left(\frac{\pi}{4}-\frac{\beta}{2}\right)\right]}\right]\right] - 2\cos\beta\left[\frac{i\beta}{2}\right. \qquad \text{(B-16)}$$

$$\left.\left. + \log\left[-i\sin\left[\left(\frac{3\pi}{4}+\frac{\chi}{2}\right)-\left(\frac{\pi}{4}-\frac{\beta}{2}\right)\right]\right]\right]\right\}$$

Using trigonometric identities and equating Z to $x + iy$ we get:

$$\frac{X}{k_1/2} = \frac{2}{\pi}\left\{\beta\sin\beta - \log\left(\tan\frac{\chi}{2}\right) + \cos\beta\,\log\left[\frac{\sin\chi}{\cos\chi+\cos\beta}\right]\right\} \qquad \text{(B-17)}$$

$$\frac{Y}{k/2} = \frac{2}{\pi}\left\{\frac{\pi}{2} - \frac{\pi}{2}\cos\beta + \sin\beta\,\log\left[\frac{\left(1+\tan\frac{\chi}{2}\right)+\left(1-\tan\frac{\chi}{2}\right)\frac{\left(1-\tan\beta/2\right)}{\left(1+\tan\beta/2\right)}}{\left(1-\tan\frac{\chi}{2}\right)+\left(1+\tan\frac{\chi}{2}\right)\frac{\left(1-\tan\beta/2\right)}{\left(1+\tan\beta/2\right)}}\right]\right\} \qquad \text{(B-18)}$$

For each value of χ between zero and $(\pi/2 - \beta/2)$ we get the coordinates x and y of a point of the free streamline. A better way of writing the equation of the streamline is to calculate χ in function of y and substitute it in the expression for x. By doing so we get:

$$\frac{\chi}{2} = \tan^{-1}\left\{\cot\frac{\beta}{2}\tanh\left[\frac{\pi}{4}\left(\frac{\bar{y}-1+\cos\beta}{\sin\beta}\right)\right]\right\} \qquad \text{(B-19)}$$

$$\text{where } \bar{y} = \frac{Y}{k_1/2}$$

$$\text{and } \bar{X} = \frac{2}{\pi}\left\{\beta\sin\beta - \log\left[\cot\frac{\beta}{2}\tanh\left[\frac{\pi}{4}\left(\frac{\bar{y}-1\cos\beta}{\sin\beta}\right)\right]\right] \right. \qquad \text{(B-20)}$$

$$\left. + \cos\beta\log\left[\frac{\sin\left[2\tan^{-1}\left[\cot\frac{\beta}{2}\tanh\left[\frac{\pi}{4}\left(\frac{\bar{y}-1+\cos\beta}{\sin\beta}\right)\right]\right]\right]}{\cos\left[2\tan^{-1}\left[\cot\frac{\beta}{2}\tanh\left[\frac{\pi}{4}\left(\frac{\bar{y}-1+\cos\beta}{\sin\beta}\right)\right]\right]\right]+\cos\beta}\right]\right\}$$

From Equation B- 20 we can tell that this free streamline has a horizontal asymptote which is

$$\overline{y} = 1 - \cos\beta$$

since $\bar{X}$ tends to infinity as $\bar{y}$ approaches this value.

In region 2 θ is between $-(2\pi-\beta)$ and -2π, let $\chi = (2\pi - \beta) - \theta$, then $\theta = -(2\pi-\beta)-\chi$ and $\chi/2$ will be between zero and $\beta/2$. Repeating the same procedure used for region 1 we get:

$$Z = \frac{k_1}{\pi}\left\{\log\left[i\cot\left(\frac{\pi}{2}+\frac{\chi}{2}-\frac{\beta}{2}\right)\right]+\cos\beta\log\left[\frac{i}{2}\left(-\sin(\chi-\beta)\right)\right]\right.$$

$$+\left(\cos\beta - i\sin\beta\right)\left[\left(\beta-\frac{\pi}{2}\right)i+\log\left[\frac{i\sin\frac{\chi}{2}}{-\cos\left(\frac{\chi}{2}+\frac{\pi}{2}-\beta\right)}\right]\right] \qquad \text{(B-21)}$$

$$\left.-2\cos\beta\left[\frac{i\beta}{2}+\log\left(i\sin\frac{\chi}{2}\right)\right]\right\}$$

Equating it to $Z = x + iy$ we get:

$$\frac{X}{k_1/2} = \frac{2}{\pi}\left\{\left(\beta-\pi\right)\sin\beta-\log\left[\tan\left(\frac{\pi}{2}+\frac{\chi}{2}-\frac{\beta}{2}\right)\right]+\cos\beta\left[\log\frac{1}{2}\right.\right.$$

$$\left.\left.+\log\left[\sin\left(\beta-\chi\right)\right]-\log\left[\sin\frac{\chi}{2}\cos\left(\frac{\chi}{2}+\frac{\pi}{2}-\beta\right)\right]\right]\right\} \qquad \text{(B-22)}$$

$$\frac{Y}{k_1/2} = \frac{2}{\pi}\left\{\frac{\pi}{2}\left(1+\cos\beta\right)-\sin\beta\log\left[\frac{\sin\frac{\chi}{2}}{\cos\left(\frac{\chi}{2}+\frac{\pi}{2}-\beta\right)}\right]\right\} \qquad \text{(B-23)}$$

then X in function of $\bar{y}$ is:

$$X = 2\cot^{-1}\left\{\cot\beta+\frac{1}{\sin\beta}\,e^{\frac{\pi}{2}\left(\frac{\bar{y}-1-\cos\beta}{\sin\beta}\right)}\right\} \qquad \text{(B-24)}$$

this free streamline also has a horizontal asymptote:

$$\bar{y} = 1 + \cos\beta$$

As the parameter θ approaches its limit, in either region 1 or 2 the free streamline will approach an asymptote. In region 1 as θ approaches $-(2\pi-\beta)$, χ will approach $(\pi-\beta)$. Let $\chi = \pi - \beta - \varepsilon$, and substitute it in Equations B-16, then take the limit as $\varepsilon \to 0$ to get the equation of the asymptote. Substituting the value of χ in the expression for X and Y we get:

as $\varepsilon \to 0$

$$\frac{X}{k_1/2} \to \frac{2}{\pi}\left\{\beta \sin\beta - \log\tan\left(\frac{\pi}{2} - \frac{\beta}{2}\right) + \cos\beta \log\frac{1}{\epsilon}\right\}$$

$$\frac{Y}{k_1/2} \to \frac{2}{\pi}\left\{\frac{\pi}{2}(1-\cos\beta) + \sin\beta\left[\log\frac{1}{\epsilon} + \log\left[\left(1+\tan\frac{\beta}{2}\right)^2 - \left(1-\tan\frac{\beta}{2}\right)^2\right]\right]\right\} \qquad \text{(B-25)}$$

Eliminate ln $1/\varepsilon$,

$$\frac{X}{k_1/2} = \frac{2}{\pi}\left\{\beta \sin\beta - \log\left(\cot\frac{\beta}{2}\right) + \cos\beta\left[\frac{\pi y}{k_1 \sin\beta} - \frac{\pi(1-\cos\beta)}{2\sin\beta}\right.\right.$$
$$\left.\left. - \log\left[\left(1+\tan\frac{\beta}{2}\right)^2 - \left(1-\tan\frac{\beta}{2}\right)^2\right]\right]\right\} \qquad \text{(B-26)}$$

Repeating the same procedure in region 2, we get the equation of the asymptote in this region. As θ approaches $-(2\pi-\beta)$, χ will approach zero. Let $\chi = \varepsilon$ and substitute it in Equations B-22 and B-23.

As $\varepsilon \to 0$

$$\frac{Y}{k_1/2} \to \frac{2}{\pi}\left\{\frac{\pi}{2}\left(1+\cos\beta\right)+\sin\beta\left(\log\sin\beta-\log\frac{\epsilon}{2}\right)\right\} \tag{B-27}$$

$$\frac{X}{k_1/2} \to \frac{2}{\pi}\left\{(\beta-\pi)\sin\beta+\log\tan\frac{\beta}{2}+\cos\beta\left[\log\frac{1}{2}+2\log\sin\beta-\log\left(\frac{\epsilon}{2}\right)\right]\right\}$$

Eliminate ln $\varepsilon/2$

$$\frac{X}{k_1/2}=\frac{2}{\pi}\left\{(\beta-\pi)\sin\beta+\log\tan\frac{\beta}{2}\right. \tag{B-28}$$

$$\left.+\cos\beta\left[\log\frac{1}{2}+2\log\sin\beta+\frac{\pi Y}{k_1\sin\beta}-\frac{\pi}{2}\frac{(1+\cos\beta)}{\sin\beta}-\log\sin\beta\right]\right\}$$

The next step will be to find the x distance from the stagnation point to the centerline of the jet. To do so we have to find the intersections of the asymptote with the x axis and add to it the length of the projected radius on the x-axis. (See Figure B-3.)

This distance from the stagnation point to the centerline of the jet is denoted by C, and is equal to

$$C = a + b$$

or

$$C = d - b$$

a is found by setting y equal to zero in Equation B-26, i.e.,

$$a=\frac{k_1}{\pi}\left\{\beta\sin\beta-\log\left(\cot\frac{\beta}{2}\right)+\cos\beta\left[-\frac{\pi}{2}\frac{(1-\cos\beta)}{\sin\beta}\right.\right. \tag{B-29}$$

$$\left.\left.-\log\left[\left(1+\tan\frac{\beta}{2}\right)^2-\left(1-\tan\frac{\beta}{2}\right)^2\right]\right]\right\}$$

and b is expressed as

$$b = \frac{k_1}{2\sin\beta} \tag{B-30}$$

Then C becomes

$$c = \frac{k_1}{\pi}\left\{-\frac{\pi}{2\sin\beta} + \beta\sin\beta - \log\left(\cot\frac{\beta}{2}\right) + \cos\beta\left[-\frac{\pi}{2}\frac{(1-\cos\beta)}{\sin\beta} - \log\left(\left(1+\tan\frac{\beta}{2}\right)^2 - \left(1-\tan\frac{\beta}{2}\right)^2\right)\right]\right\} \tag{B-31}$$

The other form of C, i.e, C = d - b, is used to check the correctness of Equation B-31.

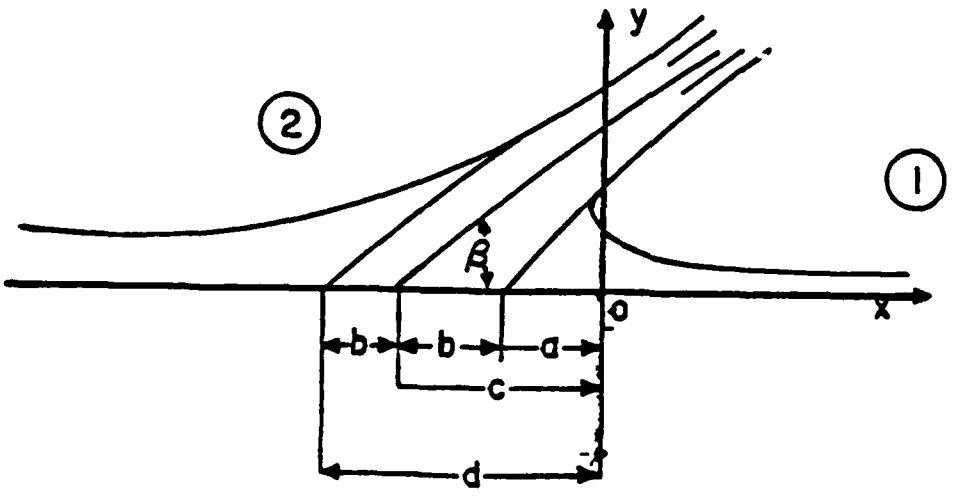

Figure B-3. The Two Regions of the Flow

APPENDIX C

APPLICATION OF LOADING MODEL TO BIRD IMPACT ON AIRCRAFT TRANSPARENCIES

APPENDIX C

APPLICATION OF LOADING MODEL TO BIRD IMPACT ON AIRCRAFT TRANSPARENCIES

Bird impacts on aircraft transparencies are different from bird impacts on other aircraft surfaces because transparencies are not rigid structures under bird loading. The transparency can significantly move and deform during a bird impact. Therefore, it is necessary to consider the windshield response. A transparency may, in general, respond to impact in two distinctly different modes which are termed locally rigid and locally deforming.

In the locally rigid case the windshield does not significantly deform in the local area of impact. See Figure C-1.

The relative velocity and impact angle change during the impact process, which results in significant changes in the magnitude and direction of the force and magnitude of the pressures excerted on the windshield.

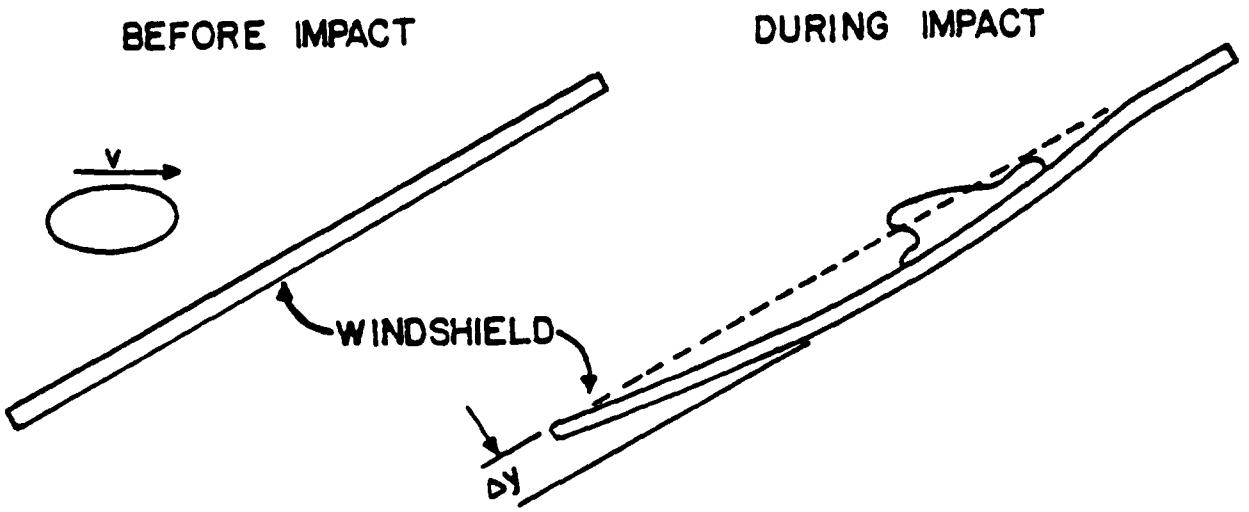

Figure C-1. Locally Rigid Windshield Response.

In the locally deforming case the local region of impact undergoes significant deformation including local changes in angle and shape. See Figure C-2. The windshield forms a pocket around the bird which results in greatly increased local loading and deformation.

In both modes the potential flow model is best fitted to sol : for the pressure distribution on the windshield during impact. Then, with the use of a structural program, deformation and velocity changes, for increments of time, can be calculated. This procedure can be repeated till the bird is consumed.

C-1 ADDITIONAL INFORMATION NEEDED FOR THE APPLICATION OF THIS LOADING MODEL TO TRANSPARENCIES

Initially the known parameters are the components of the bird velocity and the impact point coordinates. Since the surface is going to be subjected to rotation and deformation it is important to know at all times on what element the impact has occured. This will help calculating the relative velocity and non-dimensionalizing the velocities with respect to this relative velocity. The direction cosines calculated from the bird velocity components will give us the direction of the impact.

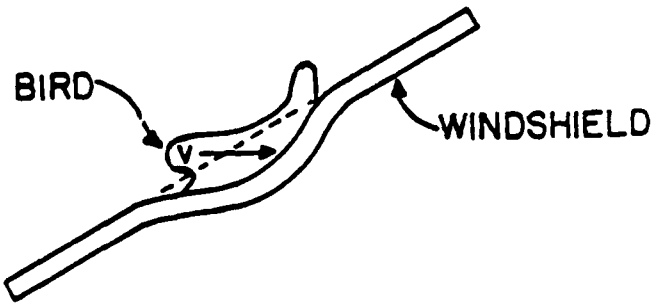

Figure C-2. Locally Deforming Windshield Response

Let VBX, VBY, and VBZ be the components of the bird velocity VR.

where: $$VR = \sqrt{VBX^2 + VBY^2 - VBZ^2}$$

then:
$$\cos\alpha = VBX/VR$$
$$\cos\beta = VBY/VR \qquad \text{(C-1)}$$
$$\cos\gamma = VBZ/VR$$

where α, β, γ are the angles that the velocity vector makes, respectively, with X, Y, and Z axis. The next step is to find the element where the impact occured. This is done by transforming the components of bird velocity and the coordinates of the impact point XI, YI, ZI into the element coordinate system. This is accomplished by using Equation 33. Then, try to find the intersection of the line, passing through the impact point with the direction cosines found earlier and the plane (X-Y) of the element.

The equation of the line is:

$$\frac{X - X'}{\cos\alpha} = \frac{Y - Y'}{\cos\beta} = \frac{Z - Z'}{\cos\gamma} \qquad \text{(C-2)}$$

where X', Y', and Z' are the coordinates of the impact point in the element coordinate system.

The intersection point is found by setting Z equal to zero. The coordinates of the intersection point are:

$$X = X' - Z' \frac{\cos\alpha}{\cos\gamma}$$
$$\text{(C-3)}$$
$$Y = Y' - Z' \frac{\cos\beta}{\cos\gamma}$$

The impact point is on the element if the sum of the angles, formed by joining the intersection point to the corner points of the quadrilateral element, equal to 360 degrees. See Figure C-3.

The onset flow still needs to be specified. It is set equal to zero outside the projection of the bird on the windshield. Within the projection it is equal to the direction cosine minus the velocity of the element, i.e.,

$$V_{\infty x} = \cos \alpha - Uxi$$
$$V_{\infty y} = \cos \beta - Uyi$$
$$V_{\infty s} = \cos \gamma - Uzi$$

where $V_{\infty x}$, $V_{\infty y}$, and $V_{\infty z}$ are the components of the velocity in the x, y, and z directions and Uxi, Uyi, and Uzi are the components of the non-dimensional velocity of the element.

A testing procedure is set to find what elements are outside the projection of the bird on the windshield, i.e., what elements have an onset flow of zero.

This is accomplished by calculating the perpendicular distance between the null point of the element and the line of impact. If this distance is greater than the radius of the bird, the element is outside the projection of the bird and the onset flow is equal to zero. Let XI, YI be the intersection point of the line of impact and the plane of the element, then the perpendicular distance D is:

$$r = \sqrt{d_1^2 + d_2^2 + d_3^2} \qquad \text{(C-6)}$$

where:

$$d_1 = \cos\gamma \cdot YI$$
$$d_2 = XI \cdot \cos\gamma \qquad \text{(C-7)}$$
$$d_3 = \cos\alpha\ (-YI) - \cos\beta\ (-XI)$$

Now we have all the information needed for the application of the loading model to bird impacts on aircraft transparencies.

REFERENCES

1. Wilbeck, J.S., "Impact Behavior of Low Strength Projectiles," AFML-TR-77-134, July 1973.

2. Allcock, A.W.R. and Collin, D.M., "The Development of a Dummy Bird for Use in Bird Strike Research," National Gas Turbine Establishment, London, England, CP-1071, June 1968.

3. Barber, J.P., Taylor, H.R., and Wilbeck, J.S., "Bird Impact Forces and Pressures on Rigid and Compliant Targets," Technical Report AFFDL-TR-77-60, May 1978.

4. Hess, J.L. and Smith, A.M.O., "Calculation of Non-Lifting Potential Flow About Arbitrary Three-Dimensional Bodies," Douglas Aircraft Company, Report No. E.S. 40622, March 1962. Also published in Journal of Ship Research, 8, No. 2, 22, September 1964, pp. 22-44.

5. Bauer, D.P. and Barber, J.P., "Experimental Investigation of Impact Pressures Caused by Gelatin Simulated Birds and Ice," University of Dayton Report UDR-TR-78-114, November 1978.

6. Milne-Thompson, L.M., Theoretical Hydrodynamics, MacMillan Company, New York, Chapter 11, 1960.

7. Schach, Von W., "Umlenkung eines Kreisformigen Flussigkeits-strahles an einer obener Platte Senkrecht Zur Stromugst-richtung," (Deflection of a Circular liquid Jet on a Plane Plate Normal to the Stream.), Ingenieur Archiv, Vol. VI, 1935, pp. 51-59.

8. Alexander, A. and Cornell, R.W., "Interactive Multi-Mode Blade Impact Analysis," NASA CR-159462, August 1978.

9. Hess, J.L. and Smith, A.M.O., "Calculation of Potential Flow about Arbitrary Bodies," Progress in Aeronautical Sciences, Vol. 8, edited by D. Kuchomann, Pergamon Press, 1967, pp. 1-138.

10. Hess, J.L., "The Problem of Three-Dimensional Lifting Potential Flow and its Solution by Means of Surface Singularity Distribution," Computer Methods in Applied Mechanics and Engineering, 4(1974), pp. 283-319.